EUROPEAN RESPIRATORY journal
FLAGSHIP SCIENTIFIC JOURNAL OF ERS

Early View

Original research article

Monocyte migration profiles define disease severity in acute COVID-19 and unique features of long COVID

Nicholas A. Scott, Laurence Pearmain, Sean B. Knight, Oliver Brand, David J. Morgan, Christopher Jagger, Sarah Harbach, Saba Khan, Halima A. Shuwa, Miriam Franklin, Verena Kästele, Thomas Williams, Ian Prise, Flora A. McClure, Pamela Hackney, Lara Smith, Madhvi Menon, Joanne E. Konkel, Criag Lawless, James Wilson, Aleaxander G. Mathioudakis, Stefan C. Stanel, Andrew Ustianowski, Gabriella Lindergard, Seema Brij, Nawar Diar Bakerly, Paul Dark, Christopher Brightling, Pilar Rivera-Ortega, Graham M. Lord, Alex Horsley, CIRCO, Karen Piper Hanley, Timothy Felton, Angela Simpson, John R. Grainger, Tracy Hussell, Elizabeth R. Mann

Please cite this article as: Scott NA, Pearmain L, Knight SB, *et al.* Monocyte migration profiles define disease severity in acute COVID-19 and unique features of long COVID. *Eur Respir J* 2023; in press (https://doi.org/10.1183/13993003.02226-2022).

Monocyte migration profiles define disease severity in acute COVID-19 and unique features of long COVID

Nicholas A. Scott[#1], Laurence Pearmain[#2,3,4], Sean B. Knight[1,5], Oliver Brand[1], David J. Morgan[1], Christopher Jagger[1], Sarah Harbach[1], Saba Khan[1], Halima A. Shuwa[1], Miriam Franklin[1], Verena Kästele[1], Thomas Williams[1], Ian Prise[1], Flora A. McClure[1], Pamela Hackney[6], Lara Smith,[6] Madhvi Menon[1], Joanne E. Konkel[1], Criag Lawless[4], James Wilson[7, 8], Aleaxander G. Mathioudakis[2,9], Stefan C. Stanel[2,9], Andrew Ustianowski[1,7], Gabriella Lindergard[7], Seema Brij[10], Nawar Diar Bakerly[5], Paul Dark[5], Christopher Brightling[11], Pilar Rivera-Ortega[2], Graham M. Lord[1], Alex Horsley[9], CIRCO[‖], Karen Piper Hanley[3,4], Timothy Felton[9], Angela Simpson[9], John R. Grainger^[1], Tracy Hussell^[1] and Elizabeth R. Mann^*[1,12].

[#]Equal contribution
^Joint senior authors
*Corresponding author

[1]Lydia Becker Institute of Immunology and Inflammation, Division of Infection, Immunity and Respiratory Medicine, School of Biological Sciences, Faculty of Biology, Medicine and Health, University of Manchester, Manchester Academic Health Science Centre, Grafton Street, Manchester, UK.

[2]North West Lung Centre, Wythenshawe Hospital, Manchester University NHS Foundation Trust, Manchester, UK.

[3]Division of Diabetes, Endocrinology and Gastroenterology, Faculty of Biology, Medicine and Health, University of Manchester, Manchester Academic Health Science Centre, Oxford Road, Manchester, UK.

[4]Wellcome Centre for Cell-Matrix Research, Faculty of Biology, Medicine and Health, Manchester Academic Health Science Centre, University of Manchester, Oxford Road, Manchester, UK.

[5]Department of Respiratory Medicine, Salford Royal NHS Foundation Trust, Stott Lane, Manchester, UK.

[6]Research Innovation, Manchester University NHS Foundation Trust, Manchester, UK.

[7]Regional Infectious Diseases Unit, North Manchester General Hospital, Manchester, UK.

[8]Department of Microbiology, Salford Royal NHS Foundation Trust, Stott Lane, Manchester, UK.

[9]Division of Infection, Immunity and Respiratory Medicine, Manchester NIHR BRC, Education and Research Centre, Wythenshawe Hospital, Manchester, UK.

[10]Department of Respiratory Medicine, Manchester Royal Infirmary, Manchester University NHS Foundation Trust, Manchester, UK.

[11]Department of Respiratory Sciences, Leicester NIHR BRC, University of Leicester, Leicester, UK.

[12]Maternal and Fetal Health Centre, Division of Developmental Biology, School of Medical Sciences, Faculty of Biology, Medicine and Health, University of Manchester, 5th Floor St. Mary's Hospital, Oxford Road, Manchester, UK.

‖ CIRCO investigators:

R. Ahmed, M. Avery, K. Birchall, R. Cairns, E. Charsley, A. Chenery, C. Chew, R. Clark, E .Connolly, K. Connolly, O. Corner, S. Dawson, L. Durrans, H. Durrington, J. Egan, C. Fox, H. Francis, S. Glasgow, N. Godfre, K.J. Gray, S. Grundy, J. Guerin, M. Iqbal, C. Hayes, E. Hardy, J. Harris, A. John, B. Jolly, S. Krishnan, S. Lui, N. Majeed, J. Mitchell, K. Moore, S. Moss, S. Murtuza Baker, R. Oliver, G. Padden, C. Parkinson, M. Phuycharoen, M. Rattray, A. Saha, B. Salcman, S. Sharma, J. Shaw, T.N. Shaw, E. Shepley, S. Stephan, R. Stephens, G. Tavernier, R. Tudge, A. Uriel, L. Wareing, R. Warren, L. Willmore, R. Wiltshire, M. Younas and S. Zriba.

ABSTRACT

Background: COVID-19 is associated with a dysregulated immune response but it is unclear how immune dysfunction contributes to the chronic morbidity persisting in many COVID-19 patients during convalescence (long COVID).

Methods: We assessed phenotypical and functional changes of monocytes in COVID-19 patients during hospitalization and up to 9 months of convalescence following COVID-19, respiratory syncytial virus (RSV) or influenza A (flu). Progressive fibrosing interstitial lung disease (PFILD) patients were included a positive control for severe, ongoing lung injury.

Results: Monocyte alterations in acute COVID-19 patients included aberrant expression of leucocyte migration molecules, continuing into convalescence (n=142) and corresponding to specific symptoms of long COVID. Long COVID patients with unresolved lung injury, indicated by sustained shortness of breath and abnormal chest radiology, were defined by high monocyte expression of chemokine receptor CXCR6 ($p<0.0001$) and adhesion molecule PSGL-1 ($p<0.01$), alongside preferential migration of monocytes towards CXCR6 ligand CXCL16 ($p<0.05$) which is abundantly expressed in the lung. Monocyte CXCR6 and lung CXCL16 were heightened in PFILD patients ($p<0.001$) confirming a role for the CXCR6-CXCL16 axis in ongoing lung injury. Conversely, monocytes from long COVID patients with ongoing fatigue exhibited sustained reduction of the prostaglandin-generating enzyme COX-2 ($p<0.01$) and CXCR2 expression ($p<0.05$). These monocyte changes were not present in RSV or flu convalescence.

Conclusions: Our data define unique monocyte signatures that define subgroups of long COVID patients, indicating a key role for monocyte migration in COVID-19 pathophysiology. Targeting these pathways may provide novel therapeutic opportunities in COVID-19 patients with persistent morbidity.

INTRODUCTION

The COVID-19 pandemic has resulted in over 664 million infections and 6.7 million deaths worldwide, to date (World Health Organisation (COVID-19) Dashboard). COVID-19 manifests with a wide range of symptoms, ranging from mild influenza-like symptoms to life threatening consequences of acute respiratory distress syndrome in severe disease [1]. There has been a significant improvement in our understanding of COVID-19 pathology from research efforts detailing changes in host immunity during SARS-CoV-2 infection, with key alterations in myeloid cells of the innate immune system corresponding to disease severity, incidence of intensive care admission and death [2-8].

Monocytes are released into the circulation from bone marrow, and recruited to the lung during respiratory infections, in keeping with our previous work demonstrating heightened systemic levels of monocyte-chemoattractant protein 1 (MCP-1) in COVID-19 patients and enhanced Ki67 on monocytes suggestive of rapid release from bone marrow [2]. Other early studies during the first wave of COVID-19 demonstrated enhanced monocyte infiltrates in the lungs, kidney, heart, spleen and muscle from deceased COVID-19 patients [9-11], supportive of a role for abnormal monocyte migration to peripheral tissues in COVID-19. Indeed, subsequent studies indicate severe COVID-19 associated variants are linked to chemokine receptor gene control in monocytes and macrophages [12]. A detailed understanding of the migratory properties of monocytes in COVID-19 and how they correspond to disease severity and intensive care admission would support the development of better, targeted clinical interventions.

There is now a wealth of evidence indicating that chronic morbidity persists in many COVID-19 patients during convalescence, with common long-lasting symptoms including extreme fatigue, shortness of breath, myalgia, brain fog, depression, fibrotic lung disease and pulmonary vascular disease (long COVID) [13-17]. Recent evidence demonstrates systemic inflammation is sustained in COVID-19 convalescence, with long COVID symptoms remaining at one year follow up [16] and long term activation of the innate immune system during convalescence even in non-severe patients [18]. There are currently limited treatment options for long COVID, since the development of targeted therapeutic strategies requires an in depth understanding of the underlying immunological pathophysiology.

We sought to address whether monocyte migratory signatures corresponded to acute COVID-19 disease severity and whether any persistent changes in immune profiles in convalescence were associated with long COVID symptoms. We collected blood samples as part of the Coronavirus Immune Response and Clinical Outcomes (CIRCO) study based at 4 different hospitals in Greater Manchester, UK [2], and identified key monocyte migratory signatures in acute disease that persisted into convalescence up to 9 months following hospital discharge. Unique monocyte profiles distinguished long COVID patients with shortness of breath and unresolved lung injury from those with ongoing fatigue, and from asymptomatic patients. Our data reveal sustained monocyte dysfunction as a key feature of acute and long COVID.

METHODS

Study design

Between July 2020 and January 2021, two cohorts of COVID-19 patients (acute and convalescent) were recruited from four hospitals across two trusts: Manchester University NHS Foundation Trust (MFT), Salford Royal NHS Foundation Trust (SRFT). Samples were collected through Manchester Allergy, Respiratory and Thoracic Surgery (ManARTS) Biobank (study number M2020-88; MFT) or the Northern Care Alliance Research Collection (NCARC) tissue biobank (study number NCA-009; SRFT). Ethical approval was provided by the National Research Ethics Service (REC reference 15/NW/0409, ManARTS; 18/WA/0368 for NCARC). Informed consent was provided by all study participants.

Patient inclusion and exclusion criteria were the same as in our previous study [2], with demographics and clinical information defined in the supplementary material (S.Fig.1 and S.Fig.3). Peripheral blood samples were collected within 7 days of hospital admission for acute patients, and at follow up appointments during outpatient clinics 3-9 months post discharge for convalescent patients. Healthy blood samples were obtained from frontline workers at the University of Manchester and Manchester University NHS Foundation Trust (MFT) and were examined alongside patient samples. All healthy controls tested negative for anti-Spike 1 receptor binding domain antibodies (age range 35-71; median age 50.9, 52% males).

Quantitative CT analysis

CT thorax scan images from symptomatic convalescent COVID-19 patients (breathless and/or fatigued) taken at follow up appointments at MFT (ManARTS study number M2022-119) were analysed using Lung Density Analysis™ and Lung Texture Analysis™ programmes to generate quantitative CT reports (Imbio Inc., Minneapolis, MN, USA). This generated quantitative scan reports as shown in S. Fig. 3. Further information on this technology can be found in the Imbio LDA+ user manual version 4.1.0 and the lung texture analysis user manual version 2.2.0. https://www.imbio.com/support-documentation/

Isolation of PBMCs and serum

Peripheral blood mononuclear cells (PBMCs) and serum from whole blood samples were isolated as previously described [2]. PBMCs were stained for flow cytometry, set up for

microbial stimulation assays, or stored in 10% dimethyl sulfoxide (DMSO) in fetal bovine serum (FBS) at -150°C.

Cell culture

Fresh PBMCs were stimulated with 100ng/ml lipopolysaccharide (LPS; Sigma) in the presence of Protein Transport Inhibitor cocktail (eBioscience) in RPMI containing 10% FBS, L-Glutamine, non-essential amino acids, HEPES, streptomycin and penicillin (complete media) for 3 hours at 37°C. Following stimulation, cells were washed and stained for flow cytometric analysis to determine intracellular levels of enzyme COX-2 and cytokines TNFα and IL-1β.

Trans-well migration assay

Frozen PBMCs from healthy controls, breathless and non-breathless convalescent COVID-19 patients were thawed, washed and resuspended in complete media. PBMCs were incubated at 37°C for 18 hours. PBMCs (2×10^5) were then plated in the upper wells of a 98-well cell migration/chemotaxis plate with Boyden chamber (Abcam; 5µm membrane). The lower wells contained CXCL16 (0.1, 0.5, 1µg/ml) or media only (negative control). PBMCs were left to migrate for 4 hours at 37°C. Migrated cells were counted manually using a haemocytometer.

Flow Cytometry

For surface stains (migration markers), samples were fixed with BD Cytofix (BD Biosciences) following antibody staining, prior to acquisition. For intracellular stains (TNFα, IL-1β, COX-2), the FoxP3/Transcription Factor Staining Buffer Set (eBioscience) was used. Antibodies used are listed in Table 1. All samples were acquired on an LSRFortessa flow cytometer (BD Biosciences) and analysed using FlowJo (TreeStar).

Luminex assay

Leucocyte migration markers were measured in serum using Luminex assays (R&D systems) according to manufacturer's instructions.

Statistics

Normality tests were performed on all datasets, and statistical analyses were carried out using Prism 9 Software (Graphpad). Information on statistical tests used is detailed in figure legends. In all cases, a *P* value of ≤ 0.05 was considered significant. Where no statistical difference is shown on graphs, there were no significant differences.

RESULTS

Clinical characteristics during acute COVID-19

Between 6th July and 5th November 2020, 71 acute patients were recruited during their in-patient stay for COVID-19 within 7 days of admission. All patients were stratified for maximum disease severity based on supplemental oxygen requirements (<28% FiO2 for mild disease, 28-60% FiO2 for moderate disease and >60% FiO2 or non-invasive/mechanical ventilation for severe disease). Additionally, the use of acute non-invasive ventilation in non COPD patients, invasive ventilation and admission to intensive care automatically led to classifying patients as having severe disease. The most frequent co-morbidities were hypertension, ischaemic heart disease, diabetes, asthma and other chronic pulmonary disease, although only diabetes correlated with disease severity (55% of severe COVID-19 patients were diabetic). 45% of severe cases of COVID-19 resulted in death within 30 days, with 30 day mortality, C-reactive protein and length of hospital stay all positively associated with COVID-19 disease severity (S. Fig 1).

Abnormal migratory signature in monocytes during acute COVID-19 defines disease severity

Following recruitment to sites of inflammation, monocytes contribute significantly to inflammatory disease directly or via differentiation into macrophages or dendritic cells in peripheral tissues [19, 20]. Monocyte-derived macrophages predominate in the broncho-alveolar lavage (BAL) of patients with severe COVID-19 [7], contributing to the inflammatory environment. We examined circulating monocytes for altered expression of a range of molecules involved in leucocyte migration, and for function based on their capacity to inflammatory mediators (summarised in S.Fig.2A).

By combining these differential analyses, we generated an overview of severity-specific monocyte signatures (Figure 1). Severe COVID-19 was characterised by reduced proportions of $CD14^+$ classical monocytes (gating strategy: S.Fig.2B) expressing the prostaglandin generating enzyme cyclooxygenase 2 (COX-2) and chemokine receptor CXCR2 (Figure 1, 2A, 2B), alongside enhanced expression of adhesion molecule CD62L (Figure 1, 2C) and the gut-homing integrin $\beta7$ (Itg $\beta7$: Figure 1, 2D). Patients with mild disease and a quicker recovery from COVID-19 displayed a distinctive signature and were characterised by heightened production of TNFα (Figures 1, 2E) and enhanced expression of chemokine receptor CCR8 on

monocytes (Figures 1, 2F). Chemokine receptor CXCR6, adhesion molecule PSGL1 and chemokine CCL2 on monocytes were aberrantly increased in COVID-19 patients overall but did not stratify with disease severity (Figures 1, 2G, S.Fig.2C).

There was a trend towards increased proportions of monocytes expressing the chemokine receptor associated with lymph node homing, CCR7, in acute COVID-19 but this did not reach statistical significance (Figure 2G). There was no change in monocyte expression of chemokine receptors CXCR1 or integrin VLA-4 that is used for adhesion to activated endothelium [21, 22] between COVID-19 patients and healthy controls (S.Fig.2D). Levels of CD31 (used for migration through the endothelium [23]) and CXCR4 were assessed rather than proportion of monocytes due to 100% of circulating monocytes expressing these molecules; there were no differences between COVID-19 patients and healthy controls. There was also no difference in monocyte production of IL-1β (S.Fig.2D).

These data indicate abnormal monocyte migration as a key factor in COVID-19 pathophysiology.

Defined soluble mediators involved in leucocyte migration are dysregulated in acute COVID-19

We, and others, have previously observed aberrant expression of soluble inflammatory mediators in serum from acute COVID-19 patients, in particular cytokines IL-6, IL-10 and chemokines MCP-1 and CXCL10 which were dominant in severe COVID-19 [1, 2, 24-26]. Here, we extended our analyses of serum proteins using a Luminex bead array targeted for leucocyte migration.

Serum levels of chemokines CCL5 (recruits leucocytes to sites of inflammation), CXCL2 (myeloid cell chemoattractant), and CXCL16 (binding partner for CXCR6 which is increased on monocytes in COVID-19 in Figure 2G) were increased in acute moderate/severe COVID-19 patients (Figure 3A). Soluble CD31 which inhibits CD31-mediated transendothelial migration [27] was reduced in COVID-19 patients, further supporting a role for heightened leucocyte migration into peripheral tissues in COVID-19 (Figure 3B). Adhesion molecule VCAM-1 and chemokines CXCL1 and CXCL10 were also elevated (Figure 3C) but did not stratify with disease

severity (data not shown). Serum levels of matrix metalloprotease 1 (MMP-1) that mediates interactions between monocytes and vascular endothelial cells [28] were also heightened in moderate/severe COVID-19 patients (Figure 3D).

These data further support a role for abnormal leucocyte migration into peripheral tissues in COVID-19 suggestive of abnormal interactions of monocytes with blood vessel endothelial cells.

Clinical characteristics during COVID-19 convalescence

Alongside recruitment of acute COVID-19 patients, between 14th July and 3rd December 2020, 142 patients attending out-patient follow-up between 63 and 246 days after discharge following in-patient admission for COVID-19 were recruited as convalescent COVID-19 patients (mean follow-up time: 151 days). At outpatient review patients were asked whether they are experiencing breathlessness or fatigue, and whether this was new since SARS-Cov-2 infection. If the symptom was pre-existing patients were asked if it was better, stable or worse since SARS-Cov-2 (quantified using Medical Research Council dyspnoea scale for breathlessness). Further clinical tests were performed by reviewing specialist respiratory physicians where indicated for shortness of breath and fatigue to exclude alternate pathologies, e.g echocardiograms, sleep studies, blood panels. If on review patient symptoms were felt to be attributable to other pathologies they were excluded from the analysis.

At out-patient follow up, 31% of patients continued to display abnormalities on chest radiology attributed to COVID-19 (S.Fig.3). Shortness of breath was the most common symptom of long COVID and indicates unresolved lung injury (48% of all convalescent patients; S.Fig.3). Here, we used the combination of abnormal chest radiology with shortness of breath to confirm unresolved lung injury, and indeed there was a significant association between these two parameters (S.Fig.3)). Fatigue was also a predominant symptom of long COVID (44% of all convalescent patients; S.Fig.3). Critically, shortness of breath and fatigue in convalescence did not correspond to initial disease severity during acute admission, thus in this cohort, COVID-19 severity does not explain persisting symptoms during convalescence. This information is important to consider in light of long COVID remaining a major public

health issue worldwide in 2022, despite the emergence of milder strains of SARS-CoV-2 and vaccination leading to a reduced risk of severe disease and hospitalisation.

There was a general decrease in all lung function parameters measured in convalescent COVID-19 patients overall, compared with predicted values [29] of the healthy population (S.Fig.4). Reductions in forced vital capacity (FVC), forced expiratory volume in 1 second (FEV_1) and diffusion capacity of the lungs for carbon monoxide (DLCO) compared to healthy populations (% predicted) are expected due to comorbidities associated with hospitalisation for COVID-19. For example, high BMI may reduce lung volumes (FVC) and asthma may affect air flow (FEV_1), whilst COPD and emphysema can affect the alveolar capillary membrane and alveolar volume (DLCO).

Breathless convalescent patients had lower FEV_1 than non-breathless convalescent patients, which may indicate patients within this group are experiencing greater airflow obstruction secondary to inflammation after SARS-CoV-2 infection (S.Fig.4). The small reduction in DLCO in all convalescent COVID-19 patients indicates a reduced capacity to transport oxygen into the bloodstream from the lungs. There was a strong trend towards a greater reduction in DLCO (% predicted) in patients with persisting abnormal radiology at follow up (S.Fig.4), which may be due to the contribution of persisting lung injury. This study is not sufficiently powered to explore the relationship between lung function measures. It is therefore unknown whether FEV_1 and DLCO findings represent a single, or separate mechanisms of breathlessness. The high prevalence of radiological abnormalities in breathless (44.4%) and fatigued (38.2%) compared to asymptomatic (25.2%) patients (S.Fig.3) are also suggestive of ongoing lung damage, or incomplete repair contributing to long COVID. Indeed, recent evidence indicates inflammatory mediators of tissue damage and repair in plasma associates with the severity of long COVID symptoms [16].

Other studies indicate enhanced detection of lung abnormalities in COVID-19 using non-standard imaging techniques, e.g. hyperpolarised 129 Xenon MRI [30]. To assess whether we may have missed any ongoing lung abnormalities using conventional radiology approaches, we carried out quantitative CT analysis using Lung Density Analysis™ and Lung Texture Analysis™ programmes (Imbio Inc., Minneapolis, MN, USA) to generate quantitative CT

reports of the lungs of a subset of symptomatic convalescent COVID-19 patients who displayed ongoing symptoms of breathlessness and/or fatigue at follow up (S.Fig.5). CT scans were generated and assessed in sagittal, coronal and transverse planes for satisfactory scan quality prior to segmentation and mapping of the lungs (S.Fig.5A). This automated computer analysis of lung texture provided detailed information regarding different types of lung damage such as hyperlucency, ground glass changes, reticulations and honeycombing (S.Fig.5B). This analysis also provides detailed information regarding lung damage in the context of lung density analysis with high density representing inflammation and ground glass changes, and very high density representing dense areas of inflammation or infection (S.Fig.5C).

Whilst this approach is previously untested in COVID-19 convalescence, it has predictive value for severity and outcome in acute COVID-19 [31]. Only 62.5% of our COVID-19 convalescent patients exhibited abnormal radiological findings using standard testing (S.Fig.6A), but quantitative CT analysis detected lung abnormalities in all of these assessed symptomatic patients with the most common abnormalities being ground glass changes and reticulations (S.Fig.6B) which are commonly associated with inflammatory processes. These results indicate that ongoing lung damage may be occurring in the majority of symptomatic COVID-19 patients during convalescence. We next assessed whether innate immune dysfunction corresponded to ongoing lung damage and symptoms of long COVID.

Abnormal monocyte migratory profile persists in COVID-19 convalescence and corresponds to symptoms of long COVID

The mechanisms by which monocytes may be involved in exacerbation versus resolution of lung injury are unclear, despite the key role of monocytes in the development of pulmonary fibrosis arising from failure of lung injury resolution [32]. Indeed, pro-fibrotic monocyte-derived macrophages accumulate in the lungs of severe COVID-19 patients with the same hallmarks of those in patients with idiopathic pulmonary fibrosis [33]. Here, we focused on shortness of breath alongside abnormal chest radiology indicative of unresolved lung injury and investigated whether sustained monocyte dysregulation corresponds to resolution of lung injury and long COVID.

Having shown that monocyte expression of chemokine receptor CXCR6 and adhesion molecule PSGL-1 were increased in acute COVID-19, we show here that these changes are sustained into convalescence, in particular in patients with on-going symptoms of breathlessness. Furthermore, expression of these molecules was also highest in patients with abnormal chest radiology (assessed by conventional methods; Figures 4A and 4F). Thus, increased CXCR6 and PSGL-1 on monocytes in breathless convalescent patients may be due to active monocyte recruitment in response to ongoing inflammation and injury in the lung. Indeed, CXCR6 directs migration towards chemokine CXCL16 which is expressed in the lung [34], with PSGL-1 mediating tethering and rolling on activated endothelium to facilitate migration into tissues from the bloodstream [35].

CXCR6 expression on monocytes in COVID-19 convalescence remained high in particular in patients who had severe COVID-19 during acute admission (Figures 4B) but initial acute disease severity had no impact on PSGL-1 expression COVID-19 convalescence (Figure 4G). Linear regression analysis comparing CXCR6 and PSGL1 expression against time (days post hospital discharge) revealed that convalescent COVID-19 patients showed no reduction of monocyte CXCR6 expression back to healthy control levels during the maximum time studied post hospital discharge (9 months; Figure 4C). However, there was a trend towards a very gradual decline in PSGL1 levels over time (Figure 4H).

To determine whether enhanced monocyte CXCR6 expression featured in convalescence following hospitalisation with other respiratory viruses, we assessed CXCR6 expression on monocytes isolated from patients at out-patient follow up, following in-patient admission with respiratory syncytial virus (RSV) or Influenza A (flu) with comparable mean follow up times (COVID-19: 151 days; RSV/flu: 155 days). All RSV and flu patients had pneumonitis upon hospital admission and 5/10 (50%) remained breathless at follow up (S.Fig.7 showing clinical characteristics and lung function). Compared to age-matched controls, there were no significant differences in post-RSV/Flu patients for monocyte expression of CXCR6, nor were there indications of heightened CXCR6 in those that remained short of breath at follow up (Figure 4D). As a positive control for unresolved lung injury, we assessed CXCR6 expression on monocytes from patients with progressive fibrosing interstitial lung disease (PFILD) who had severe ongoing lung inflammation and injury (S.Fig.7). Indeed, monocytes from PFILD

patients expressed heightened levels of CXCR6 (Figure 4D), akin to convalescent COVID-19 patients with unresolved lung injury. However PSGL1 levels on monocytes were unchanged in post flu/RSV patients and PFILD patients (S.Fig.8A).

To further interrogate the CXCR6-CXCL16 axis during ongoing lung injury, we characterised expression of the CXCR6 ligand CXCL16 on lung tissue sections from PFILD patients. Alongside clear evidence of structural damage and disorder, CXCL16 levels were visibly heightened in PFILD sections compared to healthy lung tissue with expression localised to PFILD damaged alveolar epithelial cells and infiltrating immune cells (Figure 4E). Thus, heightened monocyte CXCR6 is a feature of ongoing lung injury with clear evidence for dysregulated CXCR6-CXCL16 signalling. Nonetheless, the increased monocyte CXCR6 expression in the context of respiratory infections was only detected in COVID-19 patients.

Next, we ascertained whether the increased expression of CXCR6 on monocytes of convalescent COVID-19 patients with unresolved lung injury was functionally relevant to leucocyte migratory capacity. To do so, we performed a trans-well migration assay to reveal the migratory potential of peripheral blood mononuclear cells (PBMCs) towards CXCR6 ligand CXCL16 (expressed at high levels in the lung). PBMCs from convalescent breathless COVID-19 patients demonstrated an enhanced capacity to migrate towards CXCL16, compared to their non-breathless convalescent counterparts, and healthy controls (Figure 4I). Upon flow cytometric analysis of the cellular components within the migrated cells from the highest CXCL16 concentration, there was heightened monocyte migration from convalescent COVID-19 patients that were breathless (Figure 4J).

These data strongly implicate abnormal monocyte migration in long COVID pathology, in particular in those with unresolved lung injury and the most common symptom of long COVID – shortness of breath.

Defined soluble mediators involved in leucocyte migration are dysregulated in convalescent COVID-19

Having shown that several soluble inflammatory mediators were increased in the serum of acute COVID-19 patients, we now show that two of these serum proteins, MMP-1 (involved

in monocyte-endothelial cell interactions) and adhesion molecule VCAM-1, remain elevated in COVID-19 convalescence patients with breathlessness (Figures 5A and 5B). Furthermore, having demonstrated that PSGL-1 is increased on monocytes in breathless convalescent patients with unresolved lung injury (Figure 4D), we show here that serum levels of the PSGL-1 binding partner E-Selectin, which binds PSGL-1 to facilitate leucocyte-endothelial interactions, were enhanced in breathless COVID-19 convalescent COVID-19 patients (Figure 5C).

These data reveal that the dysregulated serum levels of specific mediators involved in leucocyte migration in acute COVID-19 remain elevated during COVID-19 convalescence and highlight their role in long COVID, in particular in shortness of breath. Together, these data so far suggest that targeting leucocyte migration and monocyte-endothelial interactions may be of therapeutic value in long COVID.

TNFα production by monocytes persists in COVID-19 convalescence and corresponds to resolved lung injury

We have demonstrated in previous studies during the first wave of COVID-19 that heightened TNFα production was prominent in patients with mild COVID-19 during hospitalisation, who recovered quickly [2]. Having replicated this finding in this study (samples taken during the second wave of COVID-19 in the UK), we now demonstrate that heightened monocyte production of TNFα is sustained into COVID-19 convalescence, and again corresponds to good outcome in terms of lung injury. Convalescent COVID-19 patients continued to produce aberrantly high levels of cytokine TNFα, in particular in patients with no symptoms of shortness of breath (Figure 6A). In keeping with increased TNFα production in patients with resolved lung injury, TNFα was significantly increased in patients with normal chest radiology during COVID-19 convalescence (Figure 6A). TNFα production in monocytes during convalescence did not correlated with initial disease severity during acute admission (Figure 6B), and significantly decreased over time, indicative of a return back to healthy control levels (Figure 6C).

To determine whether altered TNFα production by monocytes featured in convalescence following hospitalisation with other respiratory viruses, we assessed TNFα production by monocytes isolated from convalescent flu and RSV patients. There were no significant differences between controls and post-RSV/flu patients in monocyte production of TNFα (Figure 6D). To determine whether differences in TNFα levels were a general feature of resolved/unresolved lung injury, we assessed TNFα production from monocytes in PFILD patients with severe ongoing lung inflammation and injury. In keeping with a role for TNFα in resolving lung injury, monocytes from PFILD patients produced significantly lower levels of TNFα (Figure 6D).

The capacity of monocytes to produce cytokine IL-1β was also significantly higher in non-breathless compared to breathless patients during COVID-19 convalescence, although there was no change compared to healthy controls and no associations between IL-1β production and chest radiology (Figure 6E). There was no correlation with IL-1β production from monocytes and acute disease severity (Figure 6F) and there was a gradual decrease of IL-1β production from monocytes in COVID-19 convalescence over time (Figure 6G).

These data indicate that the capacity of monocytes to produce the cytokine TNFα corresponded to good outcome in terms of resolved lung injury (normal chest radiology and no shortness of breath). This information highlights the importance of considering cytokines individually for their use in anti-cytokine targeted therapies in COVID-19, as not all cytokines traditionally associated with inflammation may be contributing to pathology.

Distinct monocyte signatures during COVID-19 convalescence differentiate long COVID patients with chronic fatigue from those with unresolved lung injury.

Shortness of breath and fatigue are the most commonly reported symptoms of long COVID, with the identification of two distinct clusters of long COVID patients showing respiratory symptoms in one cluster and fatigue in the other [36]. Indeed, we show here that convalescent COVID-19 patients with ongoing fatigue were distinct from those with shortness of breath, displaying a different immune signature. To define a fatigue-specific immune signature, we removed long COVID patients with overlapping symptoms of both shortness of

breath and fatigue from these analyses. Thus we compared asymptomatic patients, with long COVID patients suffering from shortness of breath only (no fatigue), and patients with ongoing COVID-19-induced fatigue (no shortness of breath) to generate an overview of monocyte signatures corresponding to specific features of long COVID (Figure 7).

Having shown earlier that reduced monocyte expression of the prostaglandin-generating enzyme COX-2 and chemokine receptor CXCR2 was a feature of severe COVID-19 during acute disease, lowest in those requiring ITU care, we show here that these abnormal monocyte features are sustained into convalescence but specifically in patients with ongoing fatigue (Figures 7, 8A, 8B). Interestingly, there was no correlation of either COX-2 or CXCR2 expression in convalescence with initiate acute disease severity (Figures 8A, 8B). COX-2 expression on monocytes gradually increased over time at a slow rate whilst CXCR2 levels were not restored back to normal levels (Figures 8A, 8B), suggestive of long-term monocyte dysfunction in long COVID patients with fatigue. Despite indications of a trend towards decreased monocyte expression of chemokine receptor CXCR1 in patients with fatigue (Figure 7), there were no significant differences in monocyte expression of CXCR1 between healthy controls, and convalescent COVID-19 patients (fatigue or no fatigue; S.Fig.8B).

This differential analyses of fewer patients based on the specific symptoms of breathlessness only versus fatigue only, again confirmed that heightened TNFα production by monocytes in convalescence was restricted to patients with resolved lung injury (i.e. not breathless; Figure 8C). Monocyte production of IL-1β was higher in asymptomatic patients than those that were breathless (without fatigue; Figure 8D). These data support earlier data inclusive of all convalescent patients, demonstrating cytokine production by monocytes (TNFα in particular) is associated with good outcome in terms of resolution of lung injury (Figure 6A). However it is noteworthy that heightened monocyte production of TNFα in patients with resolved lung injury included those with ongoing fatigue (Figure 8C), raising the possibility that heightened TNFα could be involved in pathology in long COVID patients with ongoing fatigue. These data also clearly elucidate that heightened CXCR6 and PSGL-1 in convalescent COVID-19 patients with unresolved lung injury (Figures 4A and 4F) is specific to breathlessness rather than fatigue (Figures 7, 8E and 8F).

In summary, we show for the first time, that dysregulated monocyte migration corresponds to COVID-19 severity, both during acute phase and convalescence. Features of monocyte dysfunction in acute COVID-19 were sustained into convalescence with distinct monocyte signatures corresponding to the two most commonly reported symptoms of long COVID, shortness of breath and fatigue (summarised in S.Fig.8B).

DISCUSSION

The COVID-19 pandemic continues to cause devastating global disease as a result of inflammatory pathology from acute disease and persistent immune dysfunction during convalescence, contributing to long COVID which remains a worldwide public health issue. Our data implicate dysregulated monocyte migration in COVID-19 pathophysiology. It is now widely established that many patients develop long-term chronic symptoms following SARS-CoV-2 infection and critically, we now show that monocyte dysfunction in COVID-19 persists into convalescence even up to 9 months following hospital discharge, with differential monocyte signatures corresponding to specific aspects of long COVID (shortness of breath and fatigue).

We show a wide range of molecules involved in leucocyte migration aberrantly expressed on monocytes in acute and convalescent COVID-19, several associated with trans-endothelial migration to allow egress from blood vessels to enter peripheral tissues. We show increased VCAM-1 and E-Selectin levels in serum in long COVID patients with breathlessness, amongst other chemokines, further implicating involvement of the pulmonary endothelium and supporting previous studies showing increased levels of VCAM-1 and E-Selectin in acute COVID-19 [37].

The heightened expression of monocyte CXCR6 through convalescence is functionally relevant, with monocytes from breathless convalescent patients preferentially migrating towards the CXCR6 ligand CXCL16 *in vitro* and CXCL16 expressed at high levels in the lung [34]. The enhanced expression of CXCR6 on monocytes from PFILD patients and clear evidence for CXCL16 involvement in these patients is supportive of a key role for the CXCR6-CXCL16 axis in ongoing lung injury. The lack of heightened monocyte CXCR6 expression in RSV or flu convalescence may reflect difference in immune responses generated by different respiratory viruses, or may be reflective of the different aetiology and severity of patients admitted for acute COVID-19, RSV and flu. Further studies with larger cohorts of follow up flu and RSV patients are necessary to fully define differences in immune responses generated by these different viruses.

Our data show two distinct immune signatures corresponding to specific features of long COVID-19: breathlessness and fatigue. Whilst heightened monocyte CXCR6 and PSGL-1 expression defined breathless patients, reduced expression of COX-2 and CXCR2 defined those with ongoing fatigue. Our data are in keeping with studies identifying two distinct clusters of long COVID patients in a large UK cohort of 500,000, with fatigue predominating in one and respiratory symptoms in the other [36]. Importantly, changes in prostaglandin E2 levels (generated by COX-2 from conversion of arachidonic acid) have been associated with chronic fatigue syndrome [38] and targeting this eicosanoid pathway may be therapeutic benefit. Our data demonstrating low levels of CXCR2 associated with severe disease during acute COVID-19 and ongoing fatigue during convalescence support a protective role for CXCR2 in inflammation, in keeping with CXCR2 deficiency inducing an exaggerated inflammatory response associated with increased macrophage accumulation at inflamed sites [39].

The heightened monocyte TNFα production in patients with mild acute disease, and resolved lung injury during convalescence support studies indicating a role for TNFα in good outcome in mouse models of resolving lung injury by accelerating resolution of pulmonary fibrosis [40]. Indeed, we show here that monocyte TNFα production was reduced in PFILD patients who have severe, sustained ongoing lung injury. Furthermore, increased responsiveness to TLR ligation in monocytes and subsequent inflammatory cytokine production has been shown to be feature of patients who have recovered from COVID-19 [41]. This heightened TNFα production in convalescence appeared specific to COVID-19, with no change in convalescent RSV or flu patients. The heightened monocyte TNFα production in long COVID patients with resolved lung injury however included those with ongoing fatigue. Whilst it is unclear how TNFα may contribute to fatigue pathology, our data support recent studies implicating a role for TNFα in COVID-19 associated fatigue during convalescence [42].

In summary, we have identified abnormal features of circulating monocytes in COVID-19 with profound implications for our understanding of long COVID. Our data support studies demonstrating prolonged changes in innate immunity during COVID-19 convalescence [18, 41, 43, 44] and indicate abnormal monocyte migration as a key factor in COVID-19

pathophysiology during both acute disease and convalescence. Some of these molecules e.g. CXCR6 indicated no return back to healthy control levels over time. These findings have direct relevance for the current Omicron era due to the persistence of long COVID despite milder infections and the introduction of vaccination programmes worldwide. Whilst new variants may cause different degrees of antibody neutralisation and memory T cell responses due to different epitopes, we describe changes in innate immunity rather than adaptive, that correspond to ongoing symptoms of long COVID. With the underlying pathophysiology essentially unchanged, our data are highly likely to be relevant for Omicron and any future variants and subvariants. Furthermore, our PFILD data reveal changes to the CXCR6-CXCL16 axis as a broadly applicable mechanism important to the pathophysiology of ongoing lung injury which remains a feature of long COVID patients with breathlessness today. These data provide novel opportunities for therapeutic targeting in COVID-19 patients with persistent morbidity.

ACKNOWLEDGMENTS

We thank all participants and their families for their contribution, without which this study would not have been possible. This report is independent research supported by the UK Coronavirus Immunology Consortium (UK-CIC), the North West Lung Centre Charity and the NIHR Manchester Clinical Research Facility at Wythenshawe Hospital. We thank the Manchester Allergy, Respiratory and Thoracic Surgery Biobank, and we thank the Post-hospitalisation COVID-19 study (PHOSP-COVID) Collaborative Group, and the Northern Care Alliance Research Collection tissue bank for supporting this project. We thank Imbio Inc., Minneapolis, MN, USA for the Lung Density Analysis™ and Lung Texture Analysis™ programmes used to generated quantitative CT reports. The views expressed in this publication are those of the authors and not necessarily those of the NHS, the National Institute for Health Research or the Department of Health. Angela Simpson, Alex Horsley, Tim Felton, Paul Dark and Tracy Hussell are supported by the NIHR Manchester Biomedical Research Centre. Chris Brightling is supported by the NIHR Leicester Biomedical Research Centre. In addition, we would like to thank the Immunology community within the Lydia Becker Institute of Immunology and Inflammation, the Flow Cytometry Core Facility at the University of Manchester, the Manchester COVID-19 Rapid Response Group and the study participants for their contribution. **Funding:** This work was supported by The Wellcome Trust/Royal Society (ERM, 206206/Z/17/Z), The Kennedy Trust for Rheumatology Research who provided a Rapid Response Award for costs associated with the laboratory analysis of the immune response in COVID-19 patients to JRG, Medical Research Council (LP MR/R00191X/1; KPH MR/P023541/1), The Wellcome Trust (TH, 202865/Z/16/Z; 106898/A/15/Z which helped support some CIRCO members), the Lister Institute (JEK), BBSRC (JEK BB/M025977/1), and Innovate UK (KPH 40896).

Competing Interests: GL is Co-founder and Scientific Advisory Board Member of Gritstone Bio Inc., which is a public company that develops therapeutic vaccines for the treatment of cancer and infectious diseases including COVID-19. The other authors declare that they have no competing interests.

FIGURE LEGENDS

Figure 1. Summary of distinct monocyte profiles in acute COVID-19 patients.

Heatmap of indicated immune parameters by row. Each column represents average (mean) Z-scores for each parameter calculated from individual values of expression by monocytes from healthy individuals or mild, moderate or severe COVID-19 patients as separate groups. Heatmap was generated as a visual guide, using a subset of individuals from each group to include all individuals per group with results for every immune parameter analysed (i.e. individuals where samples were used for surface staining for all migration molecules, and microbial stimulation assays for cytokine and COX-2 readouts). Healthy individuals (n=25), mild COVID-19 (n=13), moderate COVID-19 (n=14) and severe COVID-19 (n=7).

Figure 2. Monocyte profiles of acute COVID-19 patients.

Summary graphs showing data from healthy individuals and all COVID-19 patients. **(A)** Graphs show frequencies of $CD14^+$ monocytes expressing COX-2 following LPS stimulation, from healthy individuals (n=32) and total acute COVID-19 patients (n=56). Patients with COVID-19 were also stratified into mild (n=23), moderate (n=20) and severe disease (n=10)**. (B)** Graphs show frequencies of $CD14^+$ monocytes expressing CXCR2 from healthy individuals (n=34) and total acute COVID-19 patients (n=66). Patients with COVID-19 were also stratified into mild (n=22), moderate (n=23) and severe disease (n=17)**. (C)** Graphs show $CD14^+$ monocyte CD62L expression levels as determined by mean fluorescence intensity (MFI) in healthy individuals (n=33) and total acute COVID-19 patients (n=65). Patients with COVID-19 were also stratified into mild (n=22), moderate (n=22) and severe disease (n=17)**. (D)** Graphs show frequencies of $CD14^+$ monocytes expressing integrin $\beta7$ (Itg $\beta7$) from healthy individuals (n=35) and total acute COVID-19 patients (n=67). Patients with COVID-19 were also stratified into mild (n=23), moderate (n=23) and severe disease (n=16)**. (E)** Graphs show frequencies of $CD14^+$ monocytes producing TNFα following LPS stimulation, from healthy individuals (n=34) and total acute COVID-19 patients (n=55). Patients with COVID-19 were also stratified into mild (n=23), moderate (n=20) and severe disease (n=10)**. (F)** Graphs show frequencies of $CD14^+$ monocytes expressing CCR8 from healthy individuals (n=33) and total acute COVID-19 patients (n=66). Patients with COVID-19 were also stratified into mild (n=22), moderate (n=23) and severe disease (n=17)**. (G)** Graphs show $CD14^+$ monocyte expression levels of PSGL-1 and frequencies of monocytes expressing CXCR6, CCL2 and CCR7 in healthy individuals (PSGL-1: n=35; CXCR6:

n=35; CCL2: n=33; CCR7: n=31) and total acute COVID-19 patients (PSGL-1: n=66; CXCR6: n=60; CCL2: n=57; CCR7: n=66). Graphs show individual patient data with bar representing mean ± standard error of the mean (A, C, E) or median ± interquartile range (B, D, F, G). Unpaired *t*-test (A, C, E: healthy versus COVID-19), Mann-Whitney test (B, D, F, G: healthy versus COVID-19), One-way ANOVA with Holm-Sidak post hoc test (A, C, E: COVID-19 severity), Kruskal Wallis with Dunn's post hoc test (B, D, F: COVID-19 severity). *$P \leq 0.05$, **$P \leq 0.01$, ***$P \leq 0.001$, ****$P \leq 0.0001$.

Figure 3. Serum profiles of acute COVID-19 patients.

Levels of systemic **(A)** CCL5, CXCL2, CXCL16, **(B)** soluble CD31, **(C)** VCAM-1, CXCL1, CXCL10 and **(D)** MMP-1 were measured in the serum from healthy individuals (n=13) and COVID-19 patients (n=24) using Luminex assays. **(A and D)** Patients with COVID-19 were also stratified into mild (n=11) and moderate/severe disease (n=13). Graphs show individual patient data with bar representing mean ± standard error of the mean. Unpaired *t*-test (B, C: healthy versus COVID-19), One-way ANOVA with Holm-Sidak post hoc test (A, D: COVID-19 severity). *$P \leq 0.05$, **$P \leq 0.01$, ***$P \leq 0.001$.

Figure 4. Monocyte migratory profiles of long COVID patients with unresolved lung injury.

(A) Graphs show frequencies of $CD14^+$ monocytes expressing CXCR6 from healthy individuals (n=35) and total convalescent COVID-19 patients (n=127). Patients with convalescent COVID-19 were also stratified into breathless (n=52), not breathless (n=71), normal radiology (n=91) and abnormal radiology (n=33). **(B)** Patients with convalescent COVID-19 were also stratified into mild (n=28), moderate (n=43) or severe disease (n=56), referring to their acute COVID-19 severity during previous hospital admission. **(C)** Correlation of CXCR6 (percentage of monocytes expressing CXCR6) with number of days since hospital discharge, in all convalescent COVID-19 patients (n=122). **(D)** Graph shows frequencies of $CD14^+$ monocytes expressing CXCR6 in a different cohort of healthy individuals (n=19), total convalescent flu/RSV patients (n=10) and total PFILD patients (n=14). Patients with convalescent flu/RSV were stratified into breathless (n=5, filled circles) and not breathless (n=5, open circles) within the same group. **(E)** Human lung tissue sections. Healthy human lung (left): alveoli can be seen with occasional CXCL16 expressing immune cells (black arrows) proximal to capillaries

(dashed lines). Right shows human idiopathic pulmonary fibrosis lung, with extracellular matrix replacing normal lung architecture. CXCL16 expressing immune cells are present within blood vessels (black arrows). CXCL16 is also seen in the epithelium of damaged alveoli and stromal cells. Scale bars represent 50 microns, counterstain toluidine blue. Abbreviations: ALV – alveoli; CAP – capillary. **(F)** Graphs show $CD14^+$ monocyte expression level of PSGL-1 as determined by mean fluorescence intensity (MFI) from healthy individuals (n=35) and total convalescent COVID-19 patients (n=130). Patients with convalescent COVID-19 were also stratified into breathless (n=54), not breathless (n=74), normal radiology (n=95) and abnormal radiology (n=32). **(G)** Patients with convalescent COVID-19 were also stratified into mild (n=30), moderate (n=43) or severe disease (n=57), referring to their acute COVID-19 severity during previous hospital admission. **(H)** Correlation of PSGL-1 (levels of expression as determined by mean fluorescence intensity) with number of days since hospital discharge, in all convalescent COVID-19 patients (n=130). **(I)** Numbers of migrated PBMCs as counted in bottom of Boyden chamber in media only (negative control), 0.1µg/ml CXCL16 ($CXCL16^{lo}$), 0.5µlg/ml CXCL16 ($CXCL16^{med}$) and 1µg/ml CXCL16 ($CXCL16^{hi}$) following 4 hour incubation, starting with $2x10^5$ cells in top chamber in all cases (healthy controls: n=10; breathless convalescent COVID-19: n=10; not breathless convalescent COVID-19: n=10). Graph shows combined patient data with mean $\pm$ S.E.M. of each group, under each condition. Comparison of groups was carried out using One-way ANOVA with repeated measures and Holm-Sidak post hoc test. **(J)** Numbers of migrated monocytes identified by flow cytometry as $CD45^+$ live $CD19^-$ $CD3^-$ $CD66b^-$ $HLA\text{-}DR^+$ $CD64^+$ $CD14^+$ from migrated cells in bottom of Boyden chamber in $CXCL16^{hi}$ conditions (1µg/ml CXCL16) (healthy controls: n=7; breathless convalescent COVID-19: n=10; not breathless convalescent COVID-19: n= 8). All graphs other than **(I)** show individual patient data with bar representing median $\pm$ interquartile range (A, B, D, F, G, J). Mann-Whitney test (A, F: healthy versus convalescent COVID-19), Kruskal Wallis with Dunn's post hoc test (A, B, D, F, G, J), Spearman's rank correlation coefficient test (C, H). $*P \leq 0.05$, $**P \leq 0.01$, $***P \leq 0.001$, $****P \leq 0.0001$.

Figure 5. Serum profiles of long COVID patients with unresolved lung injury.

Levels of systemic **(A)** MMP-1, **(B)** VCAM-1 and **(C)** E-Selectin were measured in the serum from healthy individuals (n=12) and convalescent COVID-19 patients (n=48) using Luminex

assays. Patients with convalescent COVID-19 were also stratified into breathless (MMP-1: n=19; VCAM-1: n=21; E-Selectin: n=21) and not breathless (MMP-1: n=26; VCAM-1: 28; E-Selectin: n=26). Graphs show individual patient data with bar representing mean ± standard error of the mean (C) or median ± interquartile range (A, B). Unpaired *t*-test (C: healthy versus convalescent COVID-19), Mann-Whitney test (A, B: healthy versus convalescent COVID-19), One-way ANOVA with Holm-Sidak post hoc test (C: breathlessness), Kruskal Wallis with Dunn's post hoc test (A, B: breathlessness). *$P \leq 0.05$, **$P \leq 0.01$, ***$P \leq 0.001$, ****$P \leq 0.0001$.

Figure 6. Monocyte cytokine profiles of long COVID patients with unresolved lung injury.
(A) Graphs show frequencies of $CD14^+$ monocytes producing TNFα from healthy individuals (n=33) and total convalescent COVID-19 patients (n=122). Patients with convalescent COVID-19 were also stratified into breathless (n=49), not breathless (n=67), normal radiology (n=87) and abnormal radiology (n=35). **(B)** Patients with convalescent COVID-19 were also stratified into mild (n=26), moderate (n=44) or severe disease (n=52), referring to their acute COVID-19 severity during previous hospital admission. **(C)** Correlation of TNFα (percentage of monocytes producing TNFα) with number of days since hospital discharge, in all convalescent COVID-19 patients (n=117). **(D)** Graph shows frequencies of $CD14^+$ monocytes producing TNFα in a different cohort of healthy individuals (n=19), total convalescent flu/RSV patients (n=10) and total PFILD patients (n=14). Patients with convalescent flu/RSV were stratified into breathless (n=5, filled circles) and not breathless (n=5, open circles) within the same group **(E)** Graphs show frequencies of $CD14^+$ monocytes producing IL-1β from healthy individuals (n=34) and total convalescent COVID-19 patients (n=122). Patients with convalescent COVID-19 were also stratified into breathless (n=49), not breathless (n=68), normal radiology (n=87) and abnormal radiology (n=34). **(F)** Patients with convalescent COVID-19 were also stratified into mild (n=26), moderate (n=44) or severe disease (n=52), referring to their acute COVID-19 severity during previous hospital admission. **(G)** Correlation of IL-1β (percentage of monocytes producing IL-1β) with number of days since hospital discharge, in all convalescent COVID-19 patients (n=118). All graphs show individual patient data with bar representing mean ± S.E.M. (A,B) or median ± I.Q.R. (E,F). Unpaired *t*-test (A: healthy versus convalescent COVID-19), Mann-Whitney test (E: healthy versus convalescent COVID-19), One-way ANOVA with Holm-Sidak post hoc test (A, B), Kruskal Wallis with Dunn's post hoc test (D, E, F), Pearson

correlation coefficient test (C), Spearman's rank correlation coefficient test (G). *$P \leq 0.05$, **$P \leq 0.01$, ***$P \leq 0.001$, ****$P \leq 0.0001$.

Figure 7. Summary of distinct monocyte profiles in subsets of long COVID patients.

Heatmap of indicated immune parameters by row. Each column represents average (mean) Z-scores for each parameter calculated from individual values of expression by monocytes from healthy individuals or convalescent COVID-19 patients without breathlessness or fatigue (asymptomatic), with breathlessness but not fatigue (breathless only) and with fatigue but not breathlessness (fatigue only), as separate groups. Heatmap was generated as a visual guide, using a subset of individuals from each group to include all individuals per group with results for every immune parameter analysed (i.e. individuals where samples were used for surface staining for all migration molecules, and microbial stimulation assays for cytokine and COX-2 readouts). Healthy individuals (n=25), asymptomatic (n=29), breathless only (n=13), fatigue only (n=16).

Figure 8. Monocyte profiles of long COVID patients with fatigue.

Summary graphs showing data from healthy individuals and all convalescent COVID-19 patients. **(A)** Graphs show frequencies of $CD14^+$ monocytes expressing COX-2 from healthy individuals (n=32) and total convalescent COVID-19 patients (n=121). Patients with convalescent COVID-19 were also stratified into asymptomatic (no breathlessness or fatigue: n=45), breathless only (breathless but not fatigued: n=15), fatigue only (fatigued but not breathless: n=22), and mild (n=26), moderate (n=44) or severe disease (n=52), referring to acute COVID-19 severity during previous hospital admission (for all convalescent patients). Correlation of COX-2 (percentage of monocytes expressing COX-2) with number of days since hospital discharge, in all convalescent COVID-19 patients (n=122). **(B)** Graphs show frequencies of $CD14^+$ monocytes expressing CXCR2 from healthy individuals (n=34) and total convalescent COVID-19 patients (n=133). Patients with convalescent COVID-19 were also stratified into asymptomatic (no breathlessness or fatigue: n=51), breathless only (breathless but not fatigued: n=18), fatigue only (fatigued but not breathless: n=25), and mild (n=30), moderate (n=44) or severe disease (n=59), referring to acute COVID-19 severity during previous hospital admission (for all convalescent patients). Correlation of CXCR2 (percentage of monocytes expressing CXCR2) with number of days since hospital discharge, in all

convalescent COVID-19 patients (n=128). **(C)** Graph shows frequency of $CD14^+$ monocytes producing TNFα in healthy individuals (n=33) and convalescent COVID-19 patients stratified into asymptomatic (no breathlessness or fatigue: n=45), breathless only (breathless but not fatigued: n=15) or fatigue only (fatigued but not breathless: n=23). **(D)** Graph shows frequency of $CD14^+$ monocytes producing IL-1β in healthy individuals (n=34) and convalescent COVID-19 patients stratified into asymptomatic (no breathlessness or fatigue: n=45), breathless only (breathless but not fatigued: n=15) or fatigue only (fatigued but not breathless: n=23). **(E)** Graph shows frequency of $CD14^+$ monocytes expressing CXCR6 in healthy individuals (n=35) and convalescent COVID-19 patients stratified into asymptomatic (no breathlessness or fatigue: n=45), breathless only (breathless but not fatigued: n=19) or fatigue only (fatigued but not breathless: n=22). **(F)** Graph shows $CD14^+$ monocyte levels of expression of PSGL-1 as determined by mean fluorescence intensity in healthy individuals (n=35) and convalescent COVID-19 patients stratified into asymptomatic (no breathlessness or fatigue: n=50), breathless only (breathless but not fatigued: n=18) or fatigue only (fatigued but not breathless: n=24). All graphs show individual patient data with bar representing mean $\pm$ S.E.M. (A-F). Unpaired *t*-test (A, B: healthy versus convalescent COVID-19), One-way ANOVA with Holm-Sidak post hoc test (A-F: long COVID symptoms, original severity), Pearson correlation coefficient test (A, B). *$P \leq 0.05$, **$P \leq 0.01$, ***$P \leq 0.001$, ****$P \leq 0.0001$.

REFERENCES

1. Huang C, Wang Y, Li X, Ren L, Zhao J, Hu Y, et al. Clinical features of patients infected with 2019 novel coronavirus in Wuhan, China. Lancet (London, England). 2020;395(10223):497-506; doi: 10.1016/s0140-6736(20)30183-5.
2. Mann ER, Menon M, Knight SB, Konkel JE, Jagger C, Shaw TN, et al. Longitudinal immune profiling reveals key myeloid signatures associated with COVID-19. Sci Immunol. 2020;5(51); doi: 10.1126/sciimmunol.abd6197.
3. Melms JC, Biermann J, Huang H, Wang Y, Nair A, Tagore S, et al. A molecular single-cell lung atlas of lethal COVID-19. Nature. 2021;595(7865):114-9; doi: 10.1038/s41586-021-03569-1.
4. Szabo PA, Dogra P, Gray JI, Wells SB, Connors TJ, Weisberg SP, et al. Longitudinal profiling of respiratory and systemic immune responses reveals myeloid cell-driven lung inflammation in severe COVID-19. Immunity. 2021;54(4):797-814 e6; doi: 10.1016/j.immuni.2021.03.005.
5. Schulte-Schrepping J, Reusch N, Paclik D, Bassler K, Schlickeiser S, Zhang B, et al. Severe COVID-19 Is Marked by a Dysregulated Myeloid Cell Compartment. Cell. 2020;182(6):1419-40 e23; doi: 10.1016/j.cell.2020.08.001.
6. Silvin A, Chapuis N, Dunsmore G, Goubet AG, Dubuisson A, Derosa L, et al. Elevated Calprotectin and Abnormal Myeloid Cell Subsets Discriminate Severe from Mild COVID-19. Cell. 2020;182(6):1401-18 e18; doi: 10.1016/j.cell.2020.08.002.
7. Liao M, Liu Y, Yuan J, Wen Y, Xu G, Zhao J, et al. Single-cell landscape of bronchoalveolar immune cells in patients with COVID-19. Nature medicine. 2020; doi: 10.1038/s41591-020-0901-9.
8. COMBATConsortium. A blood atlas of COVID-19 defines hallmarks of disease severity and specificity. Cell. 2022;185(5):916-38 e58; doi: 10.1016/j.cell.2022.01.012.
9. Carsana L, Sonzogni A, Nasr A, Rossi RS, Pellegrinelli A, Zerbi P, et al. Pulmonary post-mortem findings in a series of COVID-19 cases from northern Italy: a two-centre descriptive study. Lancet Infect Dis. 2020;20(10):1135-40; doi: 10.1016/S1473-3099(20)30434-5.
10. Beigmohammadi MT, Jahanbin B, Safaei M, Amoozadeh L, Khoshavi M, Mehrtash V, et al. Pathological Findings of Postmortem Biopsies From Lung, Heart, and Liver of 7 Deceased COVID-19 Patients. Int J Surg Pathol. 2020:1066896920935195; doi: 10.1177/1066896920935195.
11. Deshmukh V, Motwani R, Kumar A, Kumari C, Raza K. Histopathological observations in COVID-19: a systematic review. J Clin Pathol. 2020; doi: 10.1136/jclinpath-2020-206995.
12. Stikker BS, Stik G, van Ouwerkerk AF, Trap L, Spicuglia S, Hendriks RW, et al. Severe COVID-19-associated variants linked to chemokine receptor gene control in monocytes and macrophages. Genome Biol. 2022;23(1):96; doi: 10.1186/s13059-022-02669-z.
13. Fraser E. Long term respiratory complications of covid-19. BMJ. 2020;370:m3001; doi: 10.1136/bmj.m3001.
14. Williams FMK, Muirhead N, Pariante C. Covid-19 and chronic fatigue. BMJ. 2020;370:m2922; doi: 10.1136/bmj.m2922.

15. Greenhalgh T, Knight M, A'Court C, Buxton M, Husain L. Management of post-acute covid-19 in primary care. BMJ. 2020;370:m3026; doi: 10.1136/bmj.m3026.
16. PHOSP-Covid Collaborative Group P. Clinical characteristics with inflammation profiling of long COVID and association with 1-year recovery following hospitalisation in the UK: a prospective observational study. The Lancet Respiratory medicine. 2022; doi: 10.1016/S2213-2600(22)00127-8.
17. Sudre CH, Murray B, Varsavsky T, Graham MS, Penfold RS, Bowyer RC, et al. Attributes and predictors of long COVID. Nature medicine. 2021;27(4):626-31; doi: 10.1038/s41591-021-01292-y.
18. Phetsouphanh C, Darley DR, Wilson DB, Howe A, Munier CML, Patel SK, et al. Immunological dysfunction persists for 8 months following initial mild-to-moderate SARS-CoV-2 infection. Nature immunology. 2022;23(2):210-6; doi: 10.1038/s41590-021-01113-x.
19. Guilliams M, Mildner A, Yona S. Developmental and Functional Heterogeneity of Monocytes. Immunity. 2018;49(4):595-613; doi: 10.1016/j.immuni.2018.10.005.
20. Merad M, Martin JC. Pathological inflammation in patients with COVID-19: a key role for monocytes and macrophages. Nature reviews Immunology. 2020;20(6):355-62; doi: 10.1038/s41577-020-0331-4.
21. Meerschaert J, Furie MB. Monocytes use either CD11/CD18 or VLA-4 to migrate across human endothelium in vitro. Journal of immunology (Baltimore, Md : 1950). 1994;152(4):1915-26.
22. Meerschaert J, Furie MB. The adhesion molecules used by monocytes for migration across endothelium include CD11a/CD18, CD11b/CD18, and VLA-4 on monocytes and ICAM-1, VCAM-1, and other ligands on endothelium. Journal of immunology (Baltimore, Md : 1950). 1995;154(8):4099-112.
23. Liao F, Huynh HK, Eiroa A, Greene T, Polizzi E, Muller WA. Migration of monocytes across endothelium and passage through extracellular matrix involve separate molecular domains of PECAM-1. The Journal of experimental medicine. 1995;182(5):1337-43; doi: 10.1084/jem.182.5.1337.
24. Lucas C, Wong P, Klein J, Castro TBR, Silva J, Sundaram M, et al. Longitudinal analyses reveal immunological misfiring in severe COVID-19. Nature. 2020;584(7821):463-9; doi: 10.1038/s41586-020-2588-y.
25. Hadjadj J, Yatim N, Barnabei L, Corneau A, Boussier J, Smith N, et al. Impaired type I interferon activity and inflammatory responses in severe COVID-19 patients. Science (New York, NY). 2020;369(6504):718-24; doi: 10.1126/science.abc6027.
26. Ruan Q, Yang K, Wang W, Jiang L, Song J. Clinical predictors of mortality due to COVID-19 based on an analysis of data of 150 patients from Wuhan, China. Intensive care medicine. 2020;46(5):846-8; doi: 10.1007/s00134-020-05991-x.
27. Goldberger A, Middleton KA, Oliver JA, Paddock C, Yan HC, DeLisser HM, et al. Biosynthesis and processing of the cell adhesion molecule PECAM-1 includes production of a soluble form. J Biol Chem. 1994;269(25):17183-91.
28. Hojo Y, Ikeda U, Takahashi M, Sakata Y, Takizawa T, Okada K, et al. Matrix metalloproteinase-1 expression by interaction between monocytes and vascular endothelial cells. J Mol Cell Cardiol. 2000;32(8):1459-68; doi: 10.1006/jmcc.2000.1179.

29. Stanojevic S, Kaminsky DA, Miller M, Thompson B, Aliverti A, Barjaktarevic I, et al. ERS/ATS technical standard on interpretive strategies for routine lung function tests. Eur Respir J. 2021; doi: 10.1183/13993003.01499-2021.
30. Grist JT, Chen M, Collier GJ, Raman B, Abueid G, McIntyre A, et al. Hyperpolarized (129)Xe MRI Abnormalities in Dyspneic Patients 3 Months after COVID-19 Pneumonia: Preliminary Results. Radiology. 2021;301(1):E353-E60; doi: 10.1148/radiol.2021210033.
31. Guan X, Yao L, Tan Y, Shen Z, Zheng H, Zhou H, et al. Quantitative and semi-quantitative CT assessments of lung lesion burden in COVID-19 pneumonia. Sci Rep. 2021;11(1):5148; doi: 10.1038/s41598-021-84561-7.
32. Wynn TA, Vannella KM. Macrophages in Tissue Repair, Regeneration, and Fibrosis. Immunity. 2016;44(3):450-62; doi: 10.1016/j.immuni.2016.02.015.
33. Wendisch D, Dietrich O, Mari T, von Stillfried S, Ibarra IL, Mittermaier M, et al. SARS-CoV-2 infection triggers profibrotic macrophage responses and lung fibrosis. Cell. 2021;184(26):6243-61 e27; doi: 10.1016/j.cell.2021.11.033.
34. Morgan AJ, Guillen C, Symon FA, Huynh TT, Berry MA, Entwisle JJ, et al. Expression of CXCR6 and its ligand CXCL16 in the lung in health and disease. Clin Exp Allergy. 2005;35(12):1572-80; doi: 10.1111/j.1365-2222.2005.02383.x.
35. Xia L, Sperandio M, Yago T, McDaniel JM, Cummings RD, Pearson-White S, et al. P-selectin glycoprotein ligand-1-deficient mice have impaired leukocyte tethering to E-selectin under flow. J Clin Invest. 2002;109(7):939-50; doi: 10.1172/JCI14151.
36. Whitaker M, Elliott J, Chadeau-Hyam M, Riley S, Darzi A, Cooke G, et al. Persistent symptoms following SARS-CoV-2 infection in a random community sample of 508,707 people. medRxiv. 2021:2021.06.28.21259452; doi: 10.1101/2021.06.28.21259452.
37. Birnhuber A, Fliesser E, Gorkiewicz G, Zacharias M, Seeliger B, David S, et al. Between inflammation and thrombosis: endothelial cells in COVID-19. Eur Respir J. 2021;58(3); doi: 10.1183/13993003.00377-2021.
38. De Meirleir KL, Mijatovic T, Subramanian K, Schlauch KA, Lombardi VC. Evaluation of four clinical laboratory parameters for the diagnosis of myalgic encephalomyelitis. J Transl Med. 2018;16(1):322; doi: 10.1186/s12967-018-1696-z.
39. Dyer DP, Pallas K, Medina-Ruiz L, Schuette F, Wilson GJ, Graham GJ. CXCR2 deficient mice display macrophage-dependent exaggerated acute inflammatory responses. Sci Rep. 2017;7:42681; doi: 10.1038/srep42681.
40. Redente EF, Keith RC, Janssen W, Henson PM, Ortiz LA, Downey GP, et al. Tumor necrosis factor-alpha accelerates the resolution of established pulmonary fibrosis in mice by targeting profibrotic lung macrophages. Am J Respir Cell Mol Biol. 2014;50(4):825-37; doi: 10.1165/rcmb.2013-0386OC.
41. Brauns E, Azouz A, Grimaldi D, Xiao H, Thomas S, Nguyen M, et al. Functional reprogramming of monocytes in acute and convalescent severe COVID-19 patients. JCI insight. 2022; doi: 10.1172/jci.insight.154183.
42. Son K, Jamil R, Chowdhury A, Mukherjee M, Venegas C, Miyasaki K, et al. Circulating anti-nuclear autoantibodies in COVID-19 survivors predict long COVID symptoms. Eur Respir J. 2023;61(1); doi: 10.1183/13993003.00970-2022.
43. You M, Chen L, Zhang D, Zhao P, Chen Z, Qin EQ, et al. Single-cell epigenomic landscape of peripheral immune cells reveals establishment of trained immunity in

individuals convalescing from COVID-19. Nat Cell Biol. 2021;23(6):620-30; doi: 10.1038/s41556-021-00690-1.

44. Bohnacker S, Hartung F, Henkel F, Quaranta A, Kolmert J, Priller A, et al. Mild COVID-19 imprints a long-term inflammatory eicosanoid- and chemokine memory in monocyte-derived macrophages. Mucosal Immunol. 2022;15(3):515-24; doi: 10.1038/s41385-021-00482-8.

FIGURE 1

ACUTE DISEASE: Heatmap

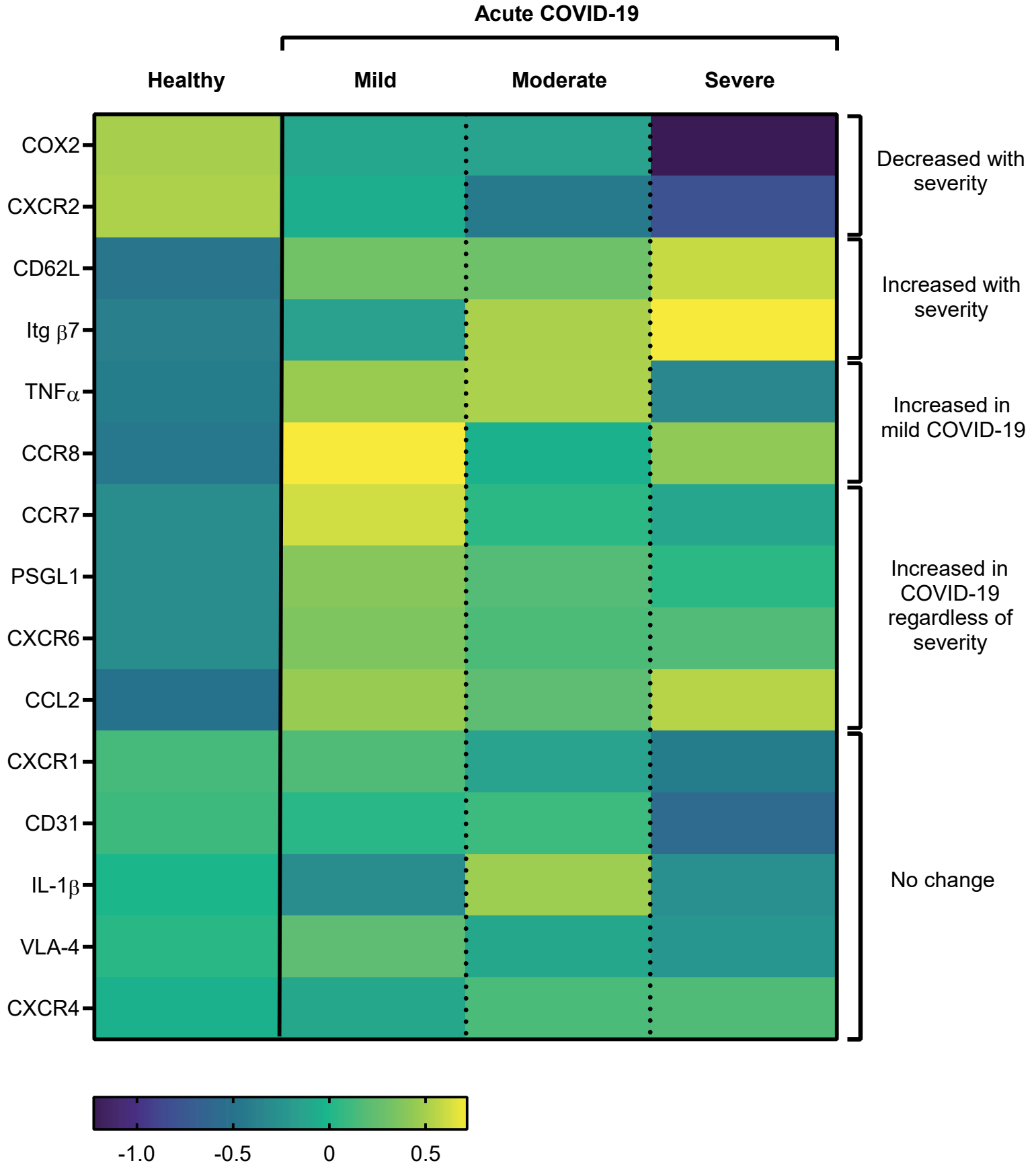

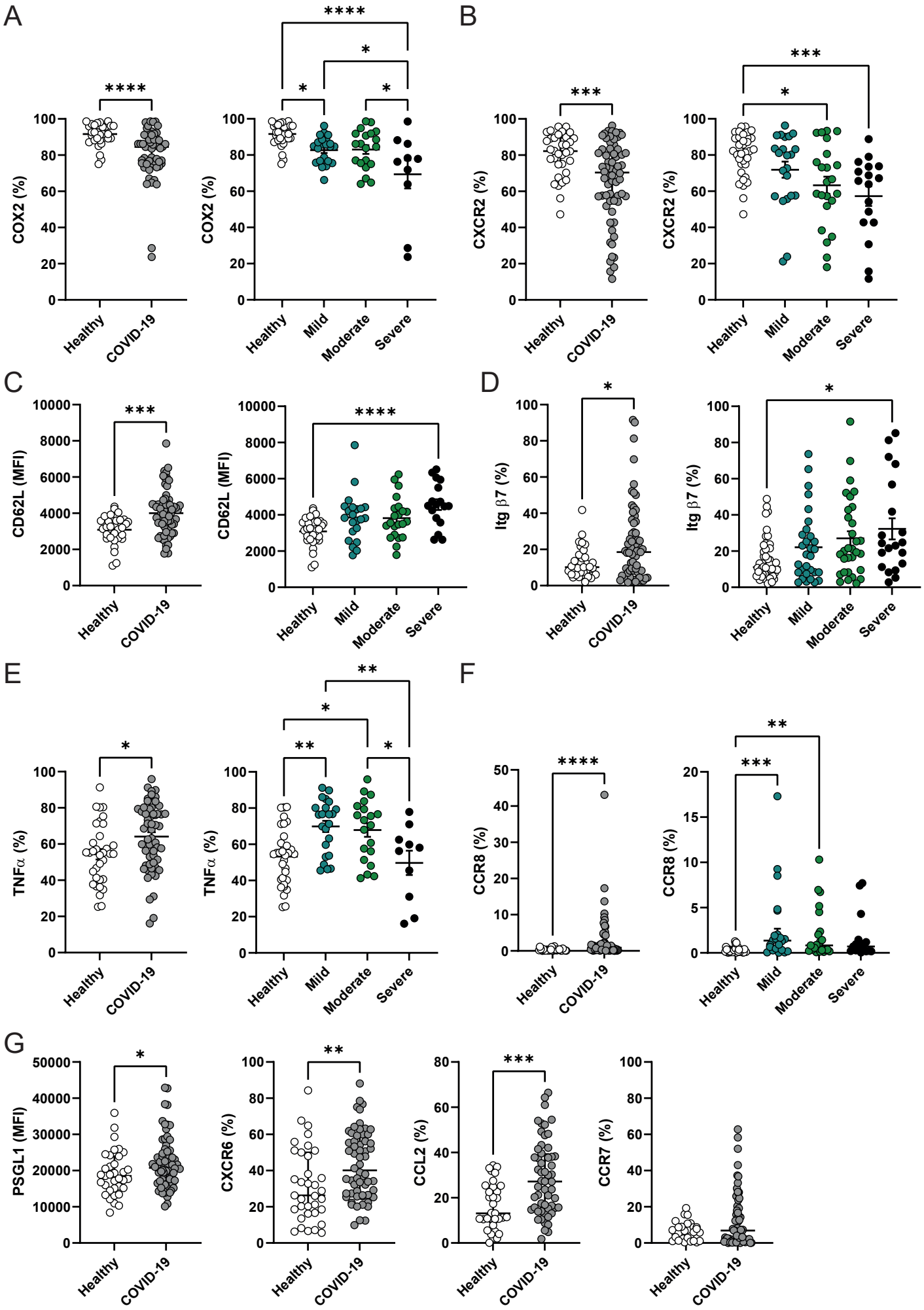
A
COX2 (%)
Healthy
COVID-19
Mild
Moderate
Severe
B
CXCR2 (%)
C
CD62L (MFI)
D
Itg β7 (%)
E
TNFα (%)
F
CCR8 (%)
G
PSGL1 (MFI)
CXCR6 (%)
CCL2 (%)
CCR7 (%)

FIGURE 3

ACUTE: Serum

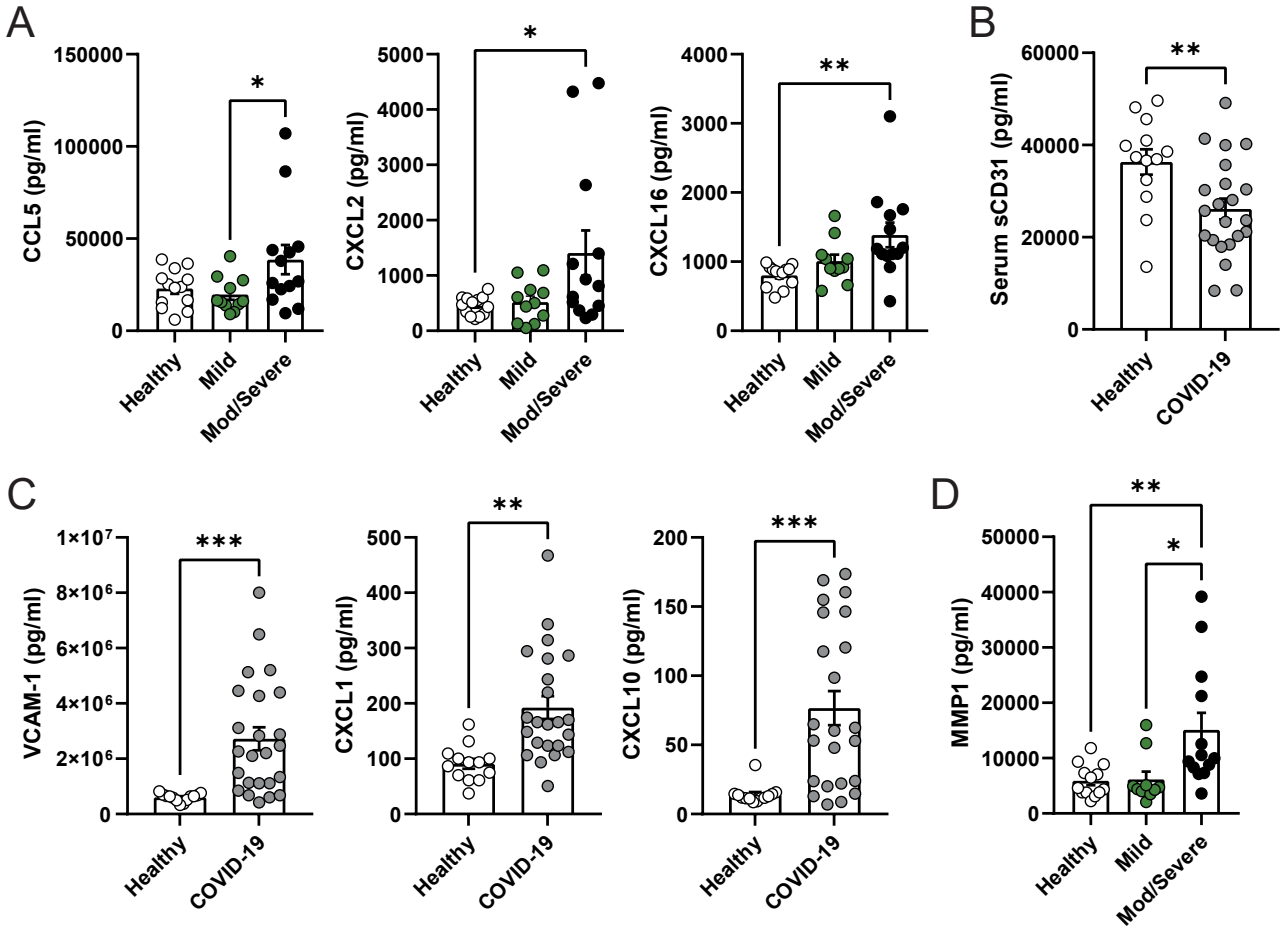

FIGURE 4

CONVALESCENCE: Breathlessness

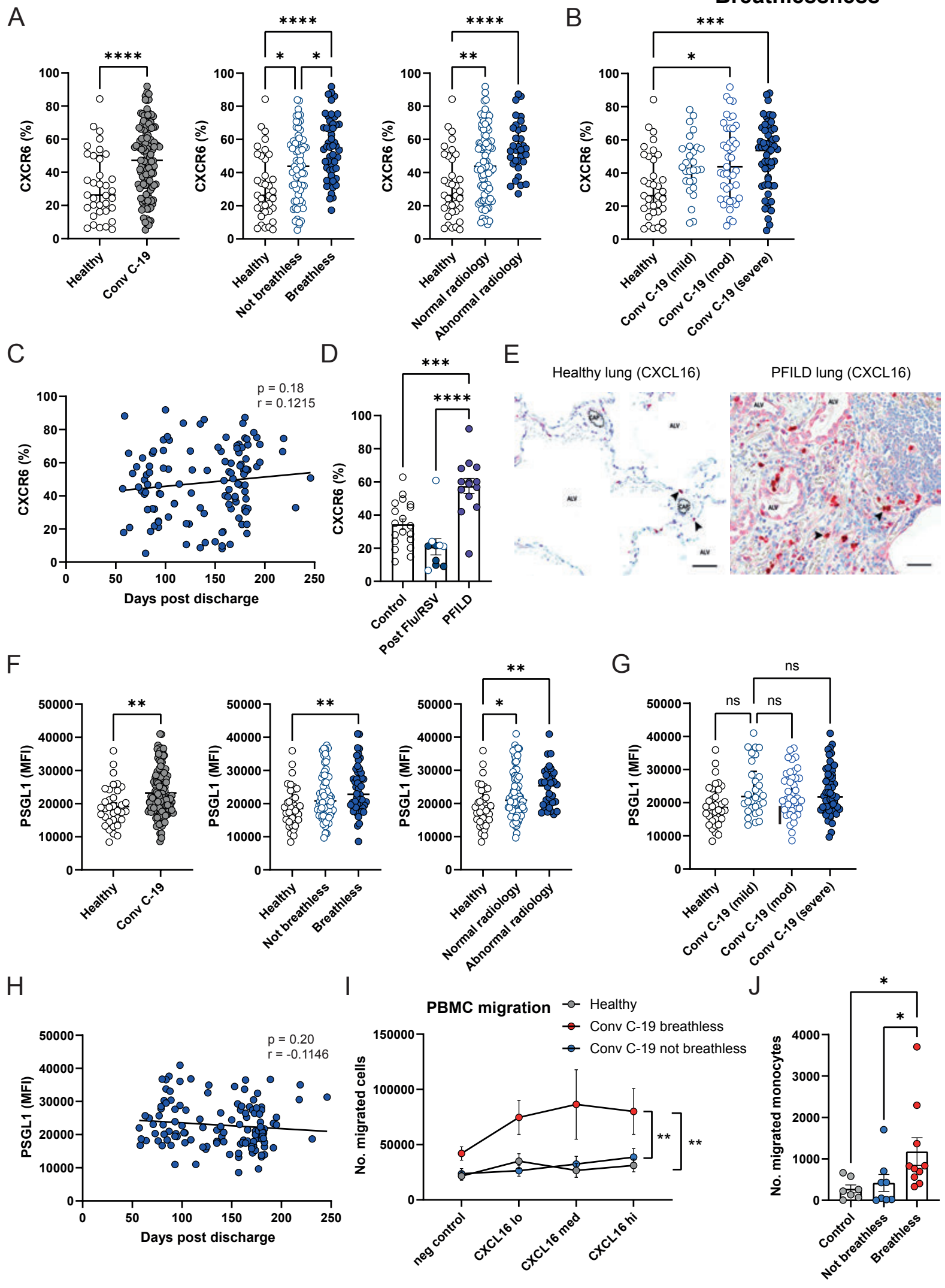

FIGURE 5

CONVALESCENCE: Serum

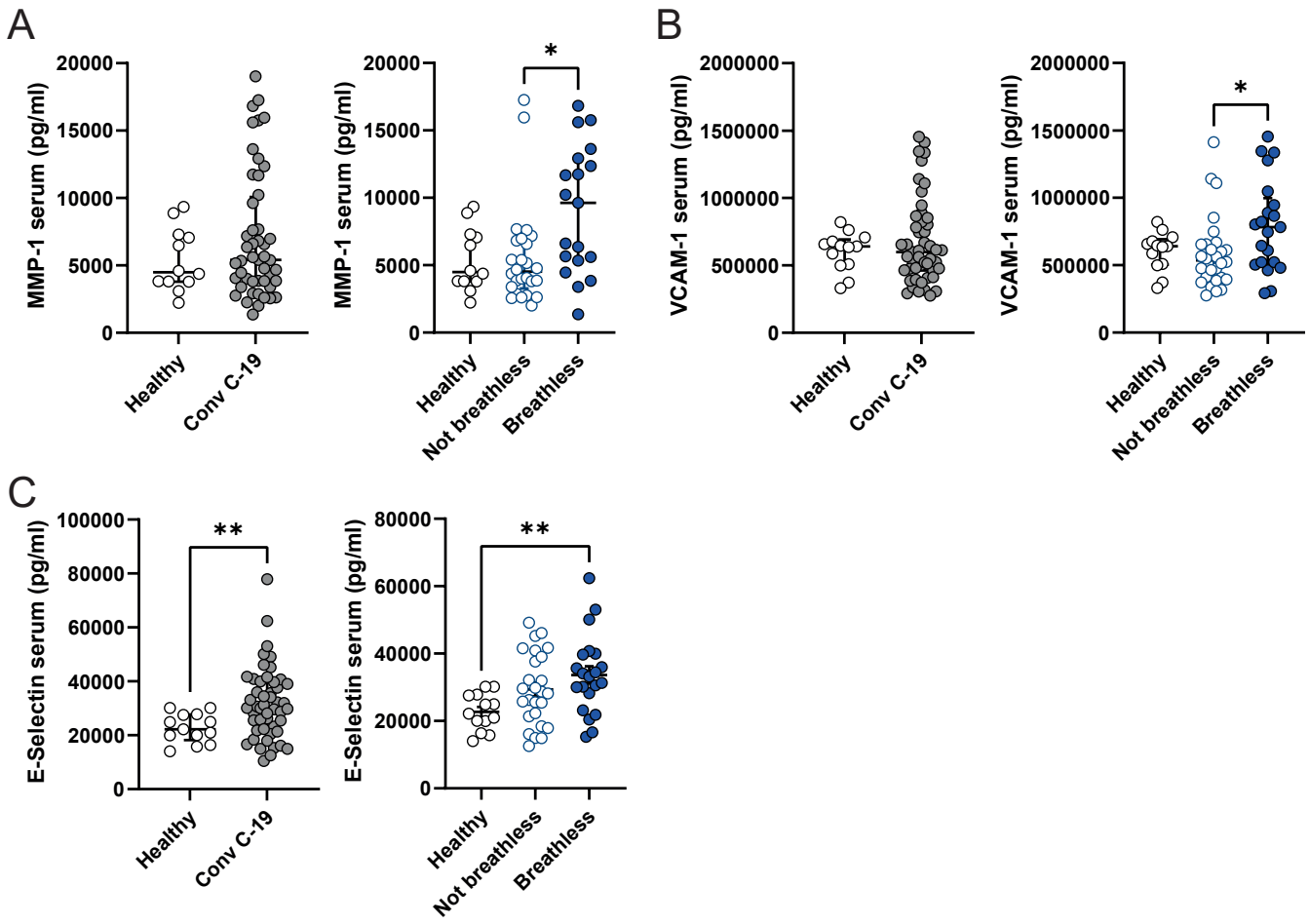

FIGURE 6

CONVALESCENCE: Breathlessness

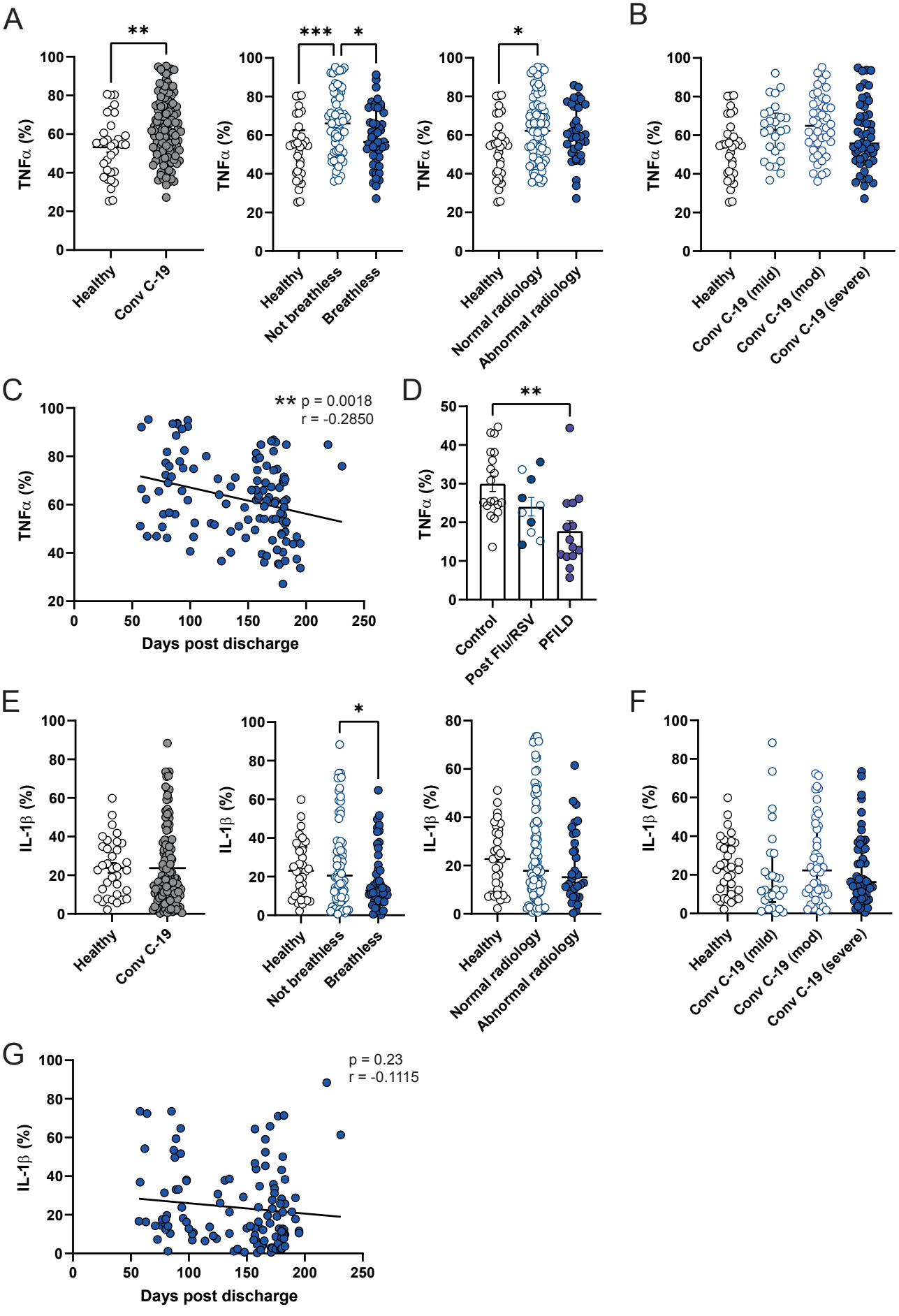

FIGURE 7

CONVALESCENCE: Immune signatures heatmap

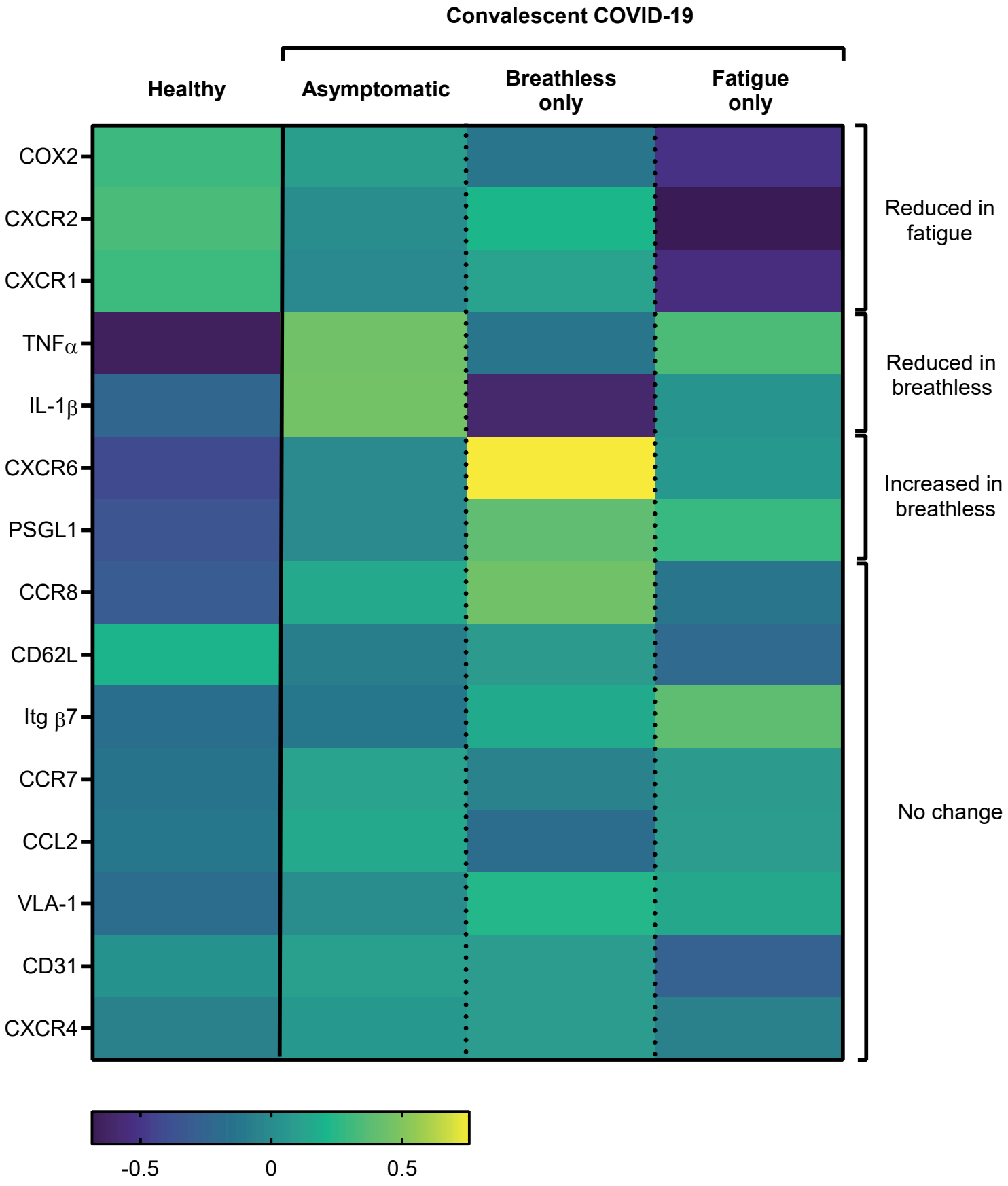

FIGURE 8

CONVALESCENCE: Fatigue

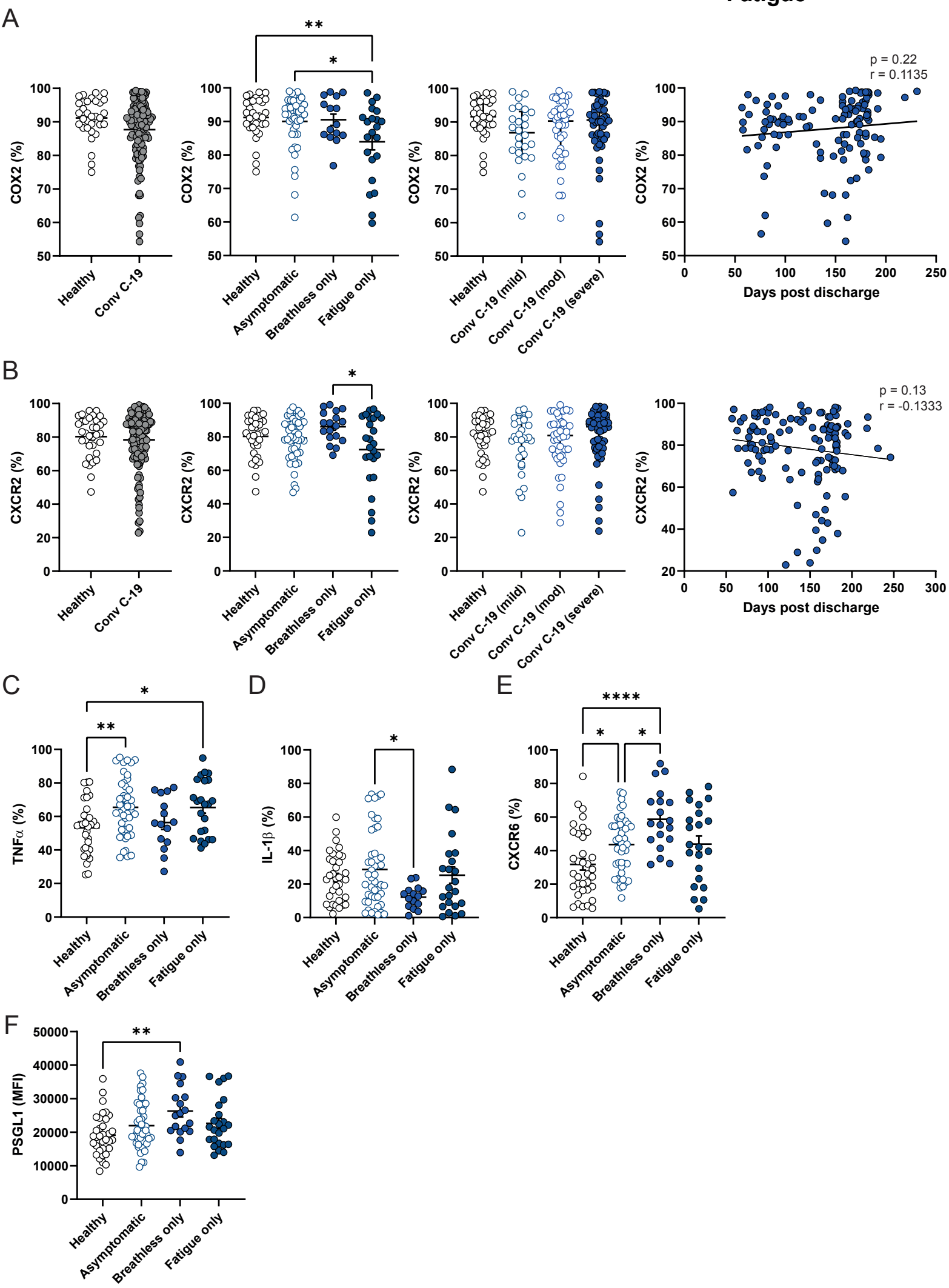

S.Fig.1 **ACUTE CHARACTERISTICS**

	All n=71	Mild n=29	Moderate N=22	Severe n=20	p value (<0.05)
Age	61.1 (2.0)	59.2 (3.7)	59.6 (3.3)	66.3 (3.1)	NS
Sex (M:F)	1.1	1.01	0.82	1.71	NS
Ethnicity (Caucasian %)	87.3 %	92.6 %	68.2 %	100 %	p<0.05
BMI	29.3 (1.1)	26.3 (2.1)	31.3 (2.2)	31.2 (1.8)	NS
Hypertension	41.4 %	63.2 %	50 %	40 %	NS
IHD	5.6 %	3.4 %	13.6 %	5.0 %	NS
Pulmonary[†]	16.9 %	24.1 %	9.1 %	15.0 %	NS
Asthma	22.5 %	17.2 %	27.3 %	26.3 %	NS
Diabetes	29.6 %	17.2 %	22.7 %	55.0 %	p<0.05
Bacterial infection	23.9 %	13.8 %	27.3 %	35.0 %	NS
PE	5.6 %	3.4 %	4.5 %	10.0 %	NS
AKI	8.5 %	10.3 %	0.0 %	15.0 %	NS
CRP	121.8 (12.1)	60.6 (15.3)	136.4 (21.7)	220.5 (27.2)	p<0.001
LOS (days)	23.7 (3.8)	24.4 (6.3)	13.1 (3.2)	35.9 (11.1)	p<0.001
30 day mortality (alive/deceased)	12.7 %	0.0 %	0.0 %	45.0 %	p<0.001

Supplementary Figure 1.

Acute (inpatient) cohort characteristics. Abbreviations as follow: IHD, ischaemic heart disease; BMI, body mass index; AKI, acute kidney injury; PE, pulmonary emboli; CRP, C-reactive protein; LOS, length of stay. † Pulmonary disease includes chronic pulmonary diseases excluding asthma. Values in ( ) represent standard error of the mean.

A

Marker	Category	Function
CXCR1	Chemokine receptor	Binds CXCL8/IL-8; migration to peripheral tissues via chemotaxis
CXCR2	Chemokine receptor	Binds CXCL8/IL-8; migration to peripheral tissues via chemotaxis
CXCR4	Chemokine receptor	Monocyte retention in bone marrow and infiltration of peripheral tissues
CXCR6	Chemokine receptor	Migration towards ligand CXCL16 which is expressed at high levels in the lung
CCR7	Chemokine receptor	Migration towards secondary lymphoid tissue
CCR8	Chemokine receptor	Migration towards secondary lymphoid tissue
PSGL1	Adhesion molecule	Facilitates leucocyte rolling on vascular endothelium to exit bloodstream
CD62L/L-Selectin	Adhesion molecule	Facilitates leucocyte tethering and rolling on vascular endothelium to exit bloodstream
CD31/PECAM-1	Adhesion molecule	Facilitates leucocyte migration through vascular endothelial junctions/endothelial transmigration into peripheral tissues
Integrin β7	Integrin	Dimerises with integrin α4 for leucocyte migration to mucosal tissues, towards MAdCAM-1 on mucosal epithelia, and interacts with extra-cellular matrix (ECM) components
VLA-4/Integrin α4β1	Integrin	Facilitates leucocyte interactions with vascular endothelia and ECM components for migration through endothelial and connective tissue barriers
TNFα	Inflammatory mediator	Induced by pattern recognition receptor (PRR) mediated activation of monocytes, inflammatory immune responses and tissue repair
IL-1β	Inflammatory mediator	Induced by pattern recognition receptor (PRR) mediated activation of monocytes, inflammatory immune responses and tissue repair
COX-2	Inflammatory mediator	Induced by pattern recognition receptor (PRR) mediated activation of monocytes, contributes to inflammation by generating prostaglandins from conversion of arachidonic acid.

B

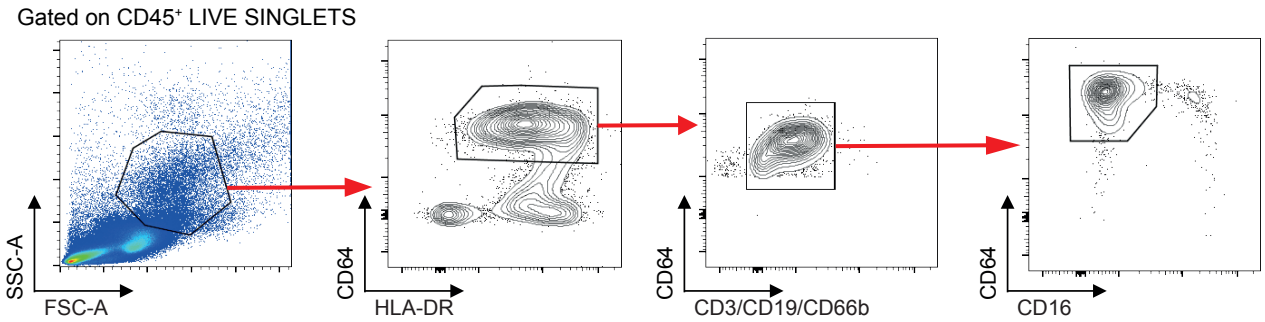

C

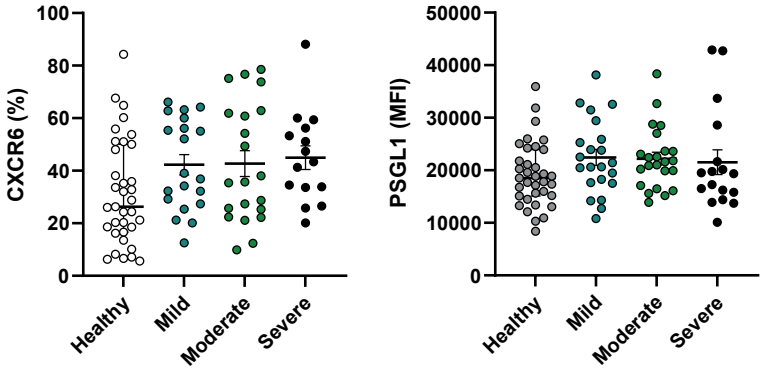

D

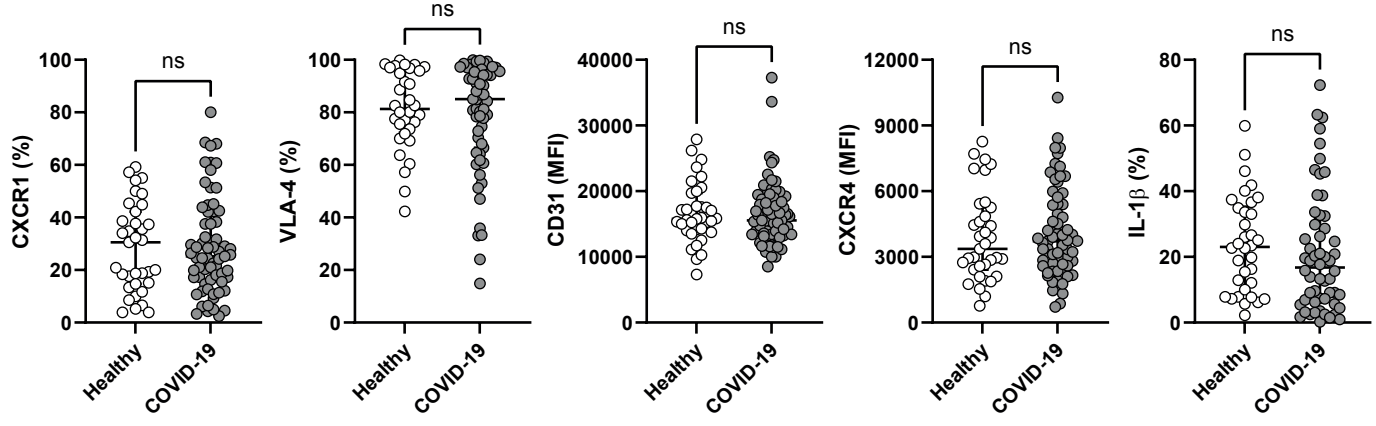

Supplementary Figure 2.

(A) Table describing functions of leucocyte migration markers and inflammatory mediators produced in response to microbial stimulation, as assessed on monocytes in COVID-19 patients. **(B)** Representative FACS plots outlining flow cytometric gating strategy used for analysis of monocytes within PBMC samples: pre-gated on live $CD45^+$ cells, circulating classical $CD14^+$ monocytes were identified as $HLA\text{-}DR^+CD64^+$ $CD3^-CD19^-CD66b^-$ $CD16^-$ cells expressing CD14. **(C)** Graphs show frequencies of $CD14^+$ monocytes expressing CXCR6 and $CD14^+$ monocyte expression level of PSGL-1 as determined by mean fluorescence intensity (MFI) from healthy individuals (n=35) and acute COVID-19 patients with mild (CXCR6: n=20; PSGL-1: n=22), moderate (CXCR6: n=21; PSGL-1: n=23) and severe (CXCR6: n=15; PSGL-1: n=17) disease. Graphs show individual patient data with bar representing median $\pm$ interquartile range. Kruskal Wallis with Dunn's post hoc test. **(D)** Graphs show frequencies of $CD14^+$ monocytes expressing CXCR1, VLA-4 and producing IL-1β and $CD14^+$ monocyte levels of expression of CD31 and CXCR4 as determined by mean fluorescence intensity in healthy individuals (CXCR1: n=35; VLA-4: n=32; CD31: n=35; CXCR4: n=35; IL-1β: n=34) and total acute COVID-19 patients (CXCR1: n=67; VLA-4: n=59; CD31: n=67; CXCR4: n=66; IL-1β: n=56). Graphs show individual patient data with bar representing mean $\pm$ standard error of the mean (CD31, CXCR4) or median $\pm$ interquartile range (CXCR1, VLA-4, IL-1β). Unpaired *t*-test (CD31, CXCR4), Mann-Whitney test (CXCR1, VLA-4, IL-1β).

S.Fig.3

CONVALESCENT CHARACTERISTICS

	All (n=142)	No breathlessness (n=70)	Shortness of breath (n=68)	No fatigue (n=73)	Fatigue (n=63)	p value (<0.05)	
						SOB	Fatigue
Mild (n=)	28	18	10	14	12		
Moderate (n=)	50	20	27	26	22		
Severe (n=)	64	32	29	33	28	NS	NS
Age	58.3 (1.1)	57.4 (1.6)	59.1 (1.5)	58.5 (1.6)	58.1 (1.5)	NS	NS
Sex (M:F)	1.73	1.69	1.77	1.68	1.72	NS	NS
Ethnicity (Caucasian %)	76.8 %	67.1 %	86.1 %	76.0 %	77.9 %	<0.01	NS
BMI	31.1 (0.5)	30.4 (0.8)	31.8 (0.6)	31.5 (0.7)	30.8 (0.7)	NS	NS
Hypertension	34.5 %	34.3 %	34.7 %	33.8 %	34.7 %	NS	NS
IHD	9.2 %	8.6 %	9.7 %	12.1 %	5.9 %	NS	NS
Pulmonary[†]	12.0 %	12.9 %	11.1 %	16.0 %	7.4 %	NS	NS
Asthma	21.8 %	17.1 %	26.4 %	18.7 %	26.5 %	NS	NS
Diabetes	12.7 %	14.3 %	11.1 %	13.3 %	11.8 %	NS	NS
Bacterial infection	14.8 %	12.9 %	16.7 %	17.3 %	13.2 %	NS	NS
PE	4.2 %	7.1 %	1.4 %	4.0 %	4.4 %	NS	NS
AKI	7.8 %	2.86 %	12.5 %	8.5 %	7.4 %	NS	NS
CRP	161.6 (9.6)	160 (13.8)	164 (15.3)	159 (15.6)	164 (13.6)	NS	NS
Length of stay	15.7 (1.8)	16.3 (3.0)	15.0 (1.9)	12.4 (1.7)	18.6 (3.0)	NS	NS
Time to follow up (days)	151.4 (3.4)	150 (4.7)	152 (5.0)	159 (5.2)	145 (4.5)	NS	<0.05
Radiology (abnormal %)	31.0 %	22.9 %	44.4 %	30.7 %	38.2 %	<0.01	NS

Supplementary Figure 3.

Convalescent COVID-19 follow up cohort lung function tests at the time of their outpatient visit. 102 of 142 patients had lung function performed. Results are presented according to the presence, or absence, of new fatigue, shortness of breath or radiological abnormality at the time of follow up. Units of measurement: FEV_1, litres/min; FVC, litres; millilitres CO/minute/mm Hg. Values in ( ) represent standard error of the mean. % predicted is a comparison to the GLI (2017) reference values.

S.Fig.4

CONVALESCENCE PROFILES

	FEV_1	FEV_1 % predicted	FVC	FVC % predicted	FEV_1/FVC %	DLCO	DLCO % predicted
All (n=102)	2.73 (0.08)	87.9 (2.14)	3.51 (0.10)	90.9 (1.71)	78.2 (0.90)	6.84 (0.35)	87.9 (1.66)
Lung function- breathlessness outcome							
No breathlessness (n=44)	2.83 (0.13)	93.2 (2.97)	3.58 (0.16)	93.7 (2.89)	79.1 (1.35)	6.64 (0.44)	86.6 (2.76)
Shortness of breath (n=58)	2.65 (0.09)	84.0 (2.97)	3.45 (0.12)	88.8 (2.08)	77.4 (1.24)	6.97 (0.54)	88.8 (2.23)
Breathlessness p value (<0.05)	NS	<0.05	NS	NS	NS	NS	NS
Lung function- fatigue outcome							
No fatigue (n=46)	2.67 (0.12)	86.5 (2.55)	3.39 (0.16)	87.3 (2.66)	79.2 (1.39)	6.08 (0.45)	94.1 (2.89)
Fatigue (n=56)	2.78 (0.09)	89.1 (3.34)	3.60 (0.12)	93.8 (2.21)	77.3 (1.21)	7.40 (0.53)	89.3 (2.01)
Fatigue p value (<0.05)	NS	NS	NS	0.06	NS	0.07	NS
Lung function-radiological outcome							
Radiology resolved (n=63)	2.75 (0.10)	87.7 (3.01)	3.56 (0.13)	92.4 (2.16)	77.3 (1.2)	7.44 (0.51)	90.0 (2.13)
Radiology abnormal (n=39)	2.69 (0.11)	88.3 (2.70)	3.40 (0.14)	88.3 (2.74)	79.6 (1.3)	5.88 (0.35)	84.6 (2.56)
Abnormal radiology p value (<0.05)	NS	NS	NS	NS	NS	<0.05	0.06

Supplementary Figure 4.

Convalescent COVID-19 follow up cohort lung function tests at the time of their outpatient visit. 102 of 142 patients had lung function performed. Results are presented according to the presence, or absence, of new fatigue, shortness of breath or radiological abnormality at the time of follow up. Units of measurement: FEV1, litres/min; FVC, litres; millilitres CO/minute/mm Hg. Values in ( ) represent standard error of the mean. % predicted is a comparison to the GLI (2017) reference values.

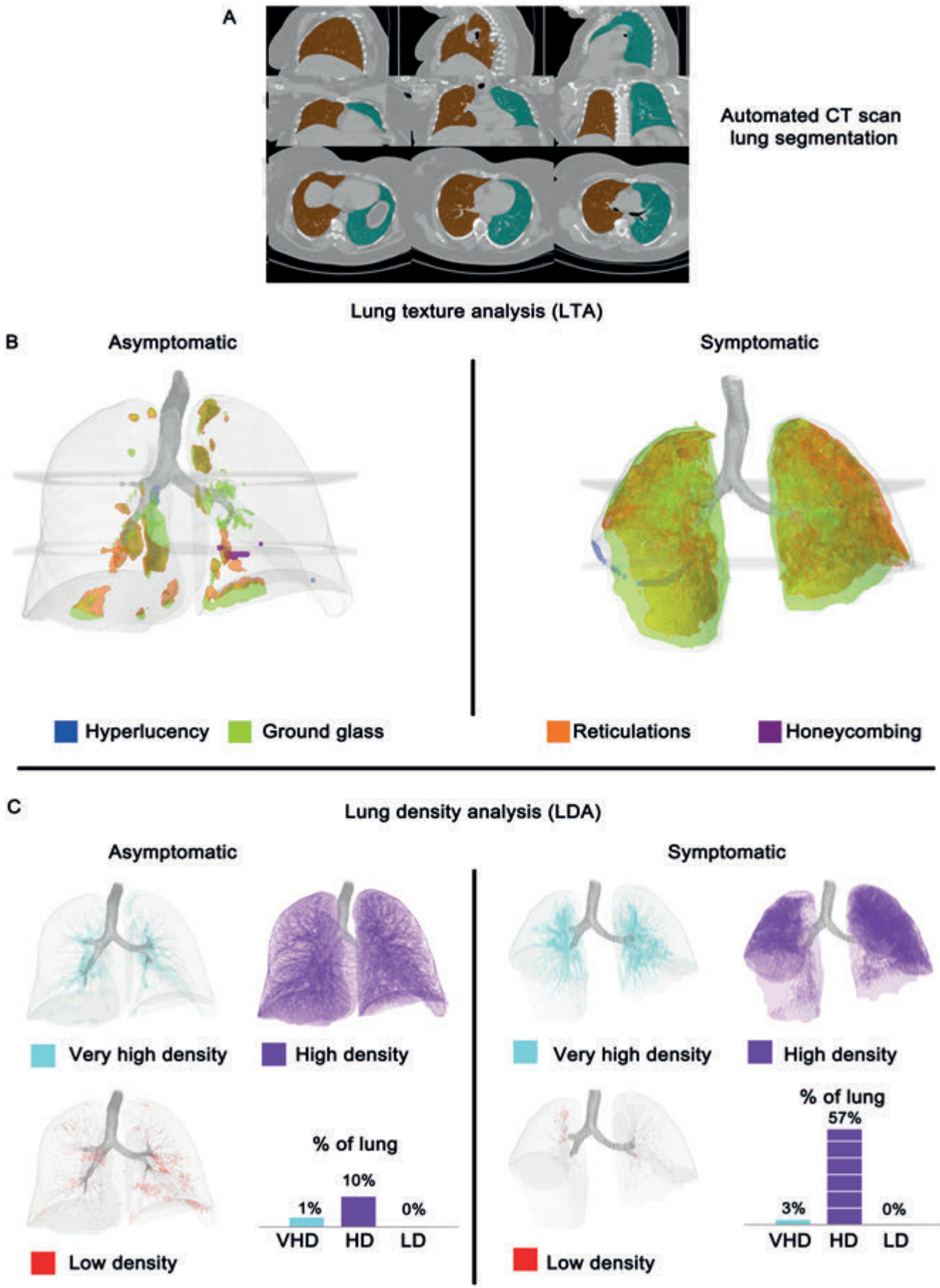
A
Automated CT scan lung segmentation
Lung texture analysis (LTA)
B
Asymptomatic
Symptomatic
Hyperlucency
Ground glass
Reticulations
Honeycombing
C
Lung density analysis (LDA)
Asymptomatic
Symptomatic
Very high density
High density
Low density
% of lung
10%
1%
0%
VHD
HD
LD
57%
3%

Supplementary Figure 5.

Quantitative CT analysis in symptomatic convalescent COVID-19 patients. CT scan images from 12 convalescent patients with breathlessness and/or fatigue, taken at outpatient follow up appointments, were analysed using lung texture analysis and lung densitometry analysis+ software algorithms (Imbio, USA). **(A)** Automated lung segmentation in sagittal (top row), coronal (middle row) and transverse (bottom row) planes. **(B)** Example of lung texture analysis in asymptomatic (no breathlessness or fatigue) and symptomatic (breathless and/or fatigued) patients enabling identification of types of lung damage including hyperlucency, ground glass changes, reticulations and honeycombing. **(C)** Example of lung density analysis in asymptomatic and symptomatic patients, enabling identification of high density and very high density representing ground glass changes and inflammation, respectively. On average, 57% of lungs of symptomatic patients displayed high density changes (ground glass changes) compared to 10% of asymptomatic patients.

A

Symptomatic post COVID-19 quantitative CT thorax (n=12)		
Demographics	Age (years)	58.9 (6.9)
	Sex (Male %)	62.5
	Ethnicity (% white)	75
	BMI	30.7 (3.69)
Acute data	Inpatient severity (% total) FiO_2 0.21-0.28 FiO_2 0.28-0.6 FiO_2 >0.6	Mild 12.5 Moderate 37.5 Severe 50
	CRP	166.5 (125.4)
	Length of stay (days)	18.8 (14.1)
Comorbidities	Hypertension (%)	62.5
	IHD (%)	25.0
	Chronic pulmonary disease† (%)	25
	Asthma (%)	25
	Diabetes (%)	12.5
Follow up data	Abnormal radiology at follow up (%)	62.5
	Breathless at follow up	50
	Fatigue at follow up	62.5
	Time to follow up (days)	143 (40.9)

B

Symptomatic post COVID-19 quantitative CT thorax (n=12)		
Quantitative CT Analysis	Hyperlucency, total %	0 (0, 1)
	Hyperlucency, maximum focal %	2 (0, 3.25)
	Ground glass, total %	30.5 (2, 65.8)
	Ground glass, maximum focal %	56 (4.25, 91)
	Reticulation, total %	7.5 (2.25, 13.75)
	Reticulation, maximum focal %	13 (2, 19.5)
	Honeycombing, total %	0 (0, 0)
	Honeycombing, maximum focal %	0 (0, 0)
	Low density total %	1 (0-4)
	Low density maximum focal %	0 (0-5)
	High density total %	30 (13-49)
	High density maximum focal %	39 (13-65)
	Very high density total %	2 (1-3)
	Very high density maximum total %	3 (3-5)
	CT follow-up time, days	157.8 (28.7)

Supplementary Figure 6.

(A) Convalescent COVID-19 follow up patient information for quantitative CT analysis. Abbreviations as follow: IHD, ischaemic heart disease; BMI, body mass index; CRP, C-reactive protein; † Pulmonary disease includes chronic pulmonary diseases excluding asthma. Values in ( ) represent standard error of the mean. **(B)** Different types of lung damage in 12 symptomatic convalescent COVID-19 patients as generated by automated quantitative CT analysis.

A

	Controls (n=17)	Viral (n=10)	PFILD (n=14)
Mild (n=) **Moderate (n=)** **Severe (n=)**		5 4 1	
Age	52.9 (4.4)	56 (5.7)	73.5 (1.5)
Sex (M:F)	0.47	1.0	3.67
Ethnicity (Caucasian %)	100.0	60.0	92.9
BMI	25.0 (0.86)	29.8 (3.4)	31.3 (2.1)
Hypertension	11.8 %	20.0 %	53.8 %
IHD	0.0 %	10.0 %	14.3 %
Pulmonary†	35.3 %	30.0 %	42.9 %
Asthma	0.0 %	40.0 %	21.4 %
Diabetes	0.0 %	20.0 %	14.3 %
CRP		47.2 (13.6)	
Length of stay (days)		6.7 (2.3)	
Time to follow up (days)		155.1 (7.8)	
Breathless (%)	0.0	50.0	100.0
Fatigue (%)	0.0	40.0	21.4

B

	FEV_1	FEV_1 % predicted	FVC	FVC % predicted	FEV_1/FVC %	DLCO	DLCO % predicted
PFILD (n=13)	2.23 (0.18)	83.3 (4.2)	2.68 (0.21)	77.8 (3.69)	87.5 (4.48)	3.51 (0.30)	50.4 (4.28)

Supplementary Figure 7.

(A) Control, viral (n=4 Influenza A, n=6 Respiratory Syncytial Virus) and progressive fibrosing interstitital lung disease (PFILD) characteristics. Abbreviations as follow: IHD, ischaemic heart disease; BMI, body mass index; CRP, C-reactive protein; LOS, length of stay. † Pulmonary disease includes chronic pulmonary diseases excluding asthma. Values in ( ) represent standard error of the mean. **(B)** PFILD lung function tests at the time of diagnosis of progressive phenotype. Units of measurement: FEV_1, litres/min; FVC, litres; millilitres CO/minute/mm Hg. Values in ( ) represent standard error of the mean. % predicted is a comparison to the GLI (2017) reference values.

S.Fig.8

STUDY OUTLINE

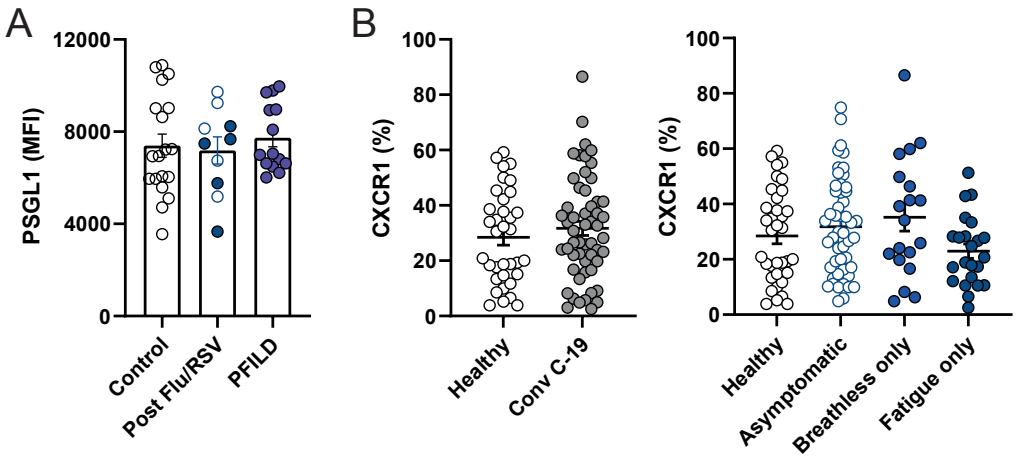

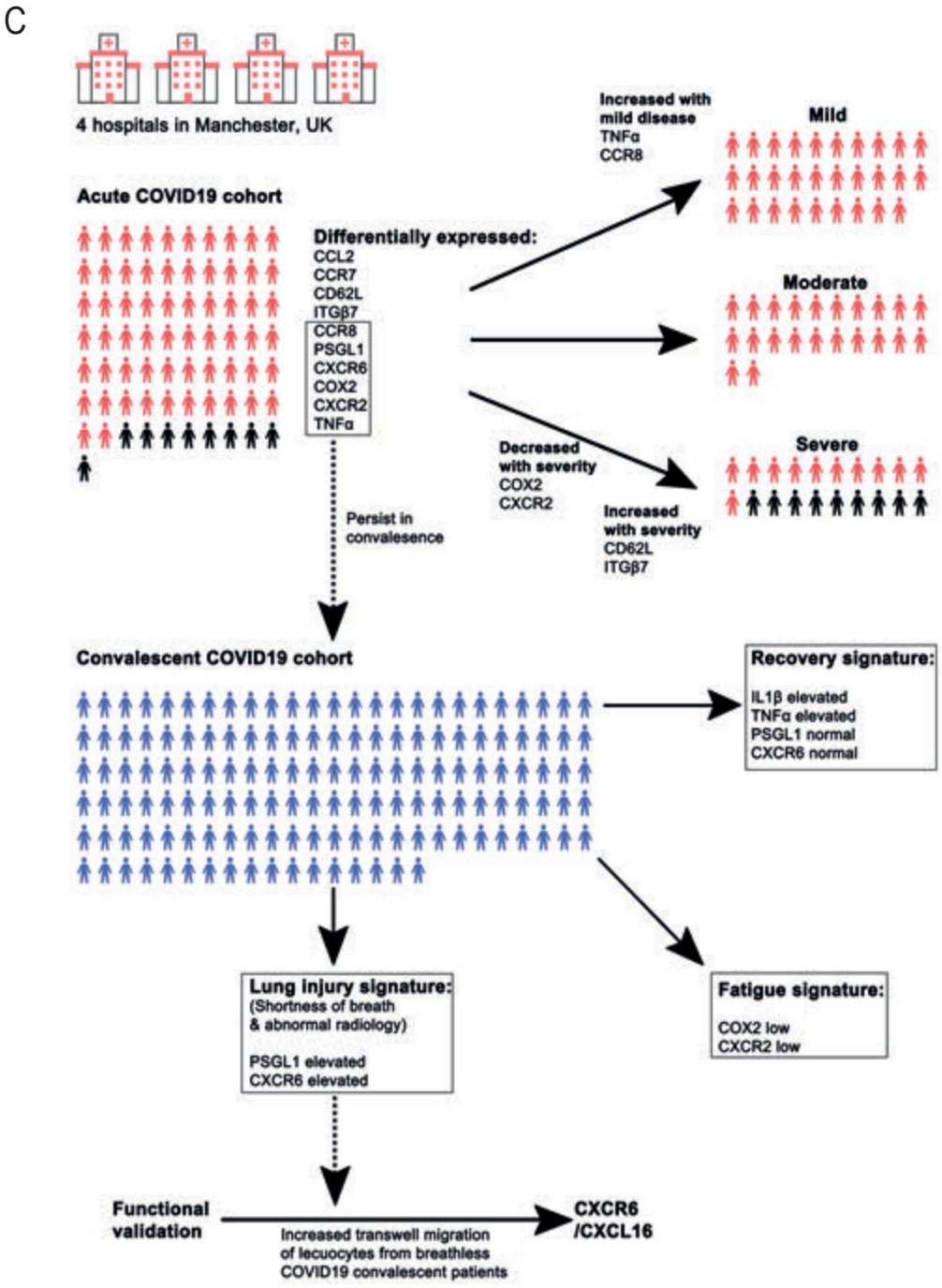

Supplementary Figure 8.

(A) Graph showing $CD14^+$ monocyte expression level of PSGL-1 as determined by mean fluorescence intensity (MFI) from healthy individuals (n=19), total convalescent flu/RSV patients (n=10) and total PFILD patients (n=14). Patients with convalescent flu/RSV were stratified into breathless (n=5, filled circles) and not breathless (n=5, open circles) within the same group. Graphs show individual patient data with bar representing median ± interquartile range. Kruskal Wallis with Dunn's post hoc test. **(B)** Graphs show frequencies of $CD14^+$ monocytes expressing CXCR1 from healthy individuals (n=35) and total convalescent COVID-19 patients (n=133). Patients with convalescent COVID-19 were also stratified into asymptomatic (no breathlessness or fatigue: n=51), breathless only (breathless but not fatigued: n=19), fatigue only (fatigued but not breathless: n=23). Graphs show individual patient data with bar representing mean ± S.E.M. Unpaired *t*-test (healthy versus convalescent COVID-19), One-way ANOVA with Holm-Sidak post hoc test (long COVID symptoms). **(C)** Summary schematic demonstrating severity-specific abnormal monocyte features in acute COVID-19 and distinct monocyte signatures corresponding to specific long COVID phenotypes.

Antibody	Clone	Company
CD45	2D1	Biolegend
CD64	10.1	Biolegend
HLA-DR	L234	Biolegend
CD3	UCHT1	Biolegend
CD19	H1B19	Biolegend
CD66b	G10F5	Biolegend
CD14	63D3	Biolegend
CD16	3G8	Biolegend
CXCR1	8F1	Biolegend
CXCR2	5E8	Biolegend
CXCR4	12G5	Biolegend
CXCR6	K041E5	Biolegend
CCR7	G043H7	Biolegend
CCR8	L263G8	Biolegend
CCL2/MCP-1	5D3-F7	Biolegend
PSGL-1	KPL-1	Biolegend
CD62L	DREG-56	Biolegend
Integrin β7	FIB504	Biolegend
VLA-4/CD49d	9F10	Biolegend
CD31/PECAM-1	WM59	Biolegend
IL-1β	H1b-98	Biolegend
TNFα	Mab11	BD Biosciences
COX-2	G10F5	BD Biosciences